



**APPLICATION OF CALCIUM LOOPING PROCESS USING CIRCULATING  
FLUIDIZED BED TECHNOLOGY FOR DECARBONIZATION OF WASTE-TO-  
ENERGY PLANTS**

Process modeling of a tail-end calcium looping process with Aspen Plus

Lappeenranta–Lahti University of Technology LUT

Master's Programme in Bioenergy System, Master's Thesis

2023

Tiia Hallikainen

Examiners: Associate Professor Jouni Ritvanen

Docent Kari Myöhänen

Supervisors: Martin Haaf, Dr.-Ing. (Sumitomo SHI FW Oy)

Nikolas Tolvanen, M.Sc. (Tech) (Sumitomo SHI FW Oy)

## ABSTRACT

Lappeenranta–Lahti University of Technology LUT

LUT School of Energy Systems

Energy Technology

Tiia Hallikainen

### **Application of calcium looping process using circulating fluidized bed technology for decarbonization of Waste-to-Energy plants**

Process modeling of a tail-end calcium looping process with Aspen Plus

Master's thesis

2023

81 pages, 20 figures, 30 tables, and 3 appendices

Examiners: Associate Professor Jouni Ritvanen, Docent Kari Myöhänen

Supervisors: Martin Haaf, Nikolas Tolvanen

Keywords: calcium looping, CaL, carbon capture, circulating fluidized bed, CFB, waste-to-energy, WtE, Aspen Plus

Reduction in fossil CO<sub>2</sub> emission is necessary to limit global warming. Integrating carbon capture and storage (CCS) technology into Waste-to-Energy (WtE) plants presents a way to reduce fossil CO<sub>2</sub> emissions or even create a net negative impact, thanks to the biogenic fraction in municipal solid waste (MSW). One suitable carbon capture process for WtE plants is calcium looping (CaL), which captures CO<sub>2</sub> from flue gases through cyclic reactions involving a limestone-based sorbent.

In this thesis, the application of CaL to decarbonize a WtE plant was investigated. The heat integration opportunities and energy penalty of the CaL process were examined via literature review. Heat and mass balances of CaL, the effect of CaL on the CO<sub>2</sub> emissions, and the effect of different calciner fuels, namely bio-pellets, wood residue, and solid recovered fuel (SRF), on process performance were evaluated based on a tail-end CaL process simulation model created in Aspen Plus.

It was noticed that implementing CaL into a WtE plant results in net negative CO<sub>2</sub> emissions with all the alternative calciner fuels that were examined. The energy penalty of the CaL may be reduced through heat integration into the host WtE plant, accomplished using external superheating or reheating. Among the alternative calciner fuels, the highest net power output for the CaL system was achieved when firing SRF in the calciner.

## TIIVISTELMÄ

Lappeenrannan–Lahden teknillinen yliopisto LUT

LUTin energijärjestelmien tiedekunta

Energiatekniikka

Tiia Hallikainen

### **Calcium looping prosessin soveltaminen kiertoleijupetitekniikkaa käyttäen jätteenpolttolaitoksien hiilidioksidipäästöjen vähentämiseen**

Loppupään calcium looping prosessin prosessimallinnus Aspen Plus ohjelmalla

Energiatekniikan diplomityö

2023

81 sivua, 20 kuvaa, 30 taulukkoa ja 3 liitettä

Tarkastajat: Apulaisprofessori Jouni Ritvanen, Dosentti Kari Myöhänen

Ohjaajat: Martin Haaf, Nikolas Tolvanen

Avainsanat: calcium looping, CaL, hiilidioksidin talteenotto, kiertoleijupeti, CFB, jätteenpoltto, Aspen Plus

Fossiilisten hiilidioksidipäästöjen vähentäminen on välttämätöntä ilmaston lämpenemisen rajoittamiseksi. Integroimalla hiilidioksidin talteenotto ja varastointi jätteenpolttolaitokseen voidaan fossiilisia hiilidioksidipäästöjä vähentää tai saavuttaa negatiiviset päästöt, sillä yhdyskuntajäte on osittain biogeenistä. Yksi soveltuva hiilidioksidin talteenottomenetelmä jätteenpolttolaitoksille on calcium looping (CaL), jonka hiilidioksidin talteenotto savukaasuista perustuu kalkkikivipohjaisen sorbentin syklisiin reaktioihin.

Tässä työssä tutkittiin CaL prosessin soveltamista jätteenpolttolaitoksen hiilidioksidipäästöjen vähentämiseen. CaL:n lämpöintegrointia sekä energiahäviötä tutkittiin kirjallisuuskatsauksessa. CaL prosessin lämpö- ja massataseita, vaikutusta hiilidioksidipäästöihin ja kalsinointireaktorissa käytettävien polttoaineiden vaikutusta prosessin suorituskykyyn tutkittiin Aspen Plus ohjelmalla luodun loppupään CaL prosessin simulointimallin avulla. Polttoaineet, joita simuloinneissa käytettiin olivat biopelletit, puujäte ja kiinteä kierrätyspolttoaine (SRF).

Työssä havaittiin, että CaL prosessin integroiminen jätteenpolttolaitokseen mahdollistaa negatiivisen päästövaikutuksen jokaisella simuloitulla polttoaineella. CaL:n aiheuttamaa energiahäviötä voidaan minimoida lämpöintegroinnilla jätteenpolttolaitokseen ulkoisen tulistuksen tai uudelleen tulistuksen avulla. Suurin nettoteho CaL prosessista saavutettiin, kun SRF polttoainetta poltettiin kalsinointireaktorissa.

## ACKNOWLEDGEMENTS

First of all, I would like to thank my supervisor Martin Haaf for the guidance throughout the thesis work. I appreciate the precise and comprehensive feedback that I got during the thesis work. I would also like to thank my other supervisor Nikolas Tolvanen whose guidance and tips related to Aspen Plus were fundamental in the development of the simulation model. I am grateful to Sumitomo SHI FW for the opportunity to do a master's thesis with this interesting and current topic.

I would like to thank my examiners Jouni Ritvanen and Kari Myöhänen for their comments and effort during the thesis work.

Lastly, I want to thank my family and friends for all the support, help, and encouragement during the thesis work and throughout my studies.

Varkaus, October 2023

Tiia Hallikainen

## SYMBOLS AND ABBREVIATIONS

### Roman characters

$c$	molar concentration	mol.%
$d$	diameter	mm
$E_{\text{carb}}$	CO <sub>2</sub> absorption efficiency	%
$E_{\text{tot}}$	total CO <sub>2</sub> capture efficiency	%
$F$	molar flow	kmol/h
$F_{\text{CO}_2}$	molar flow of CO <sub>2</sub>	kmol/h
$F_{\text{R}}$	molar flow of circulating Ca-species	kmol/h
$F_0$	molar flow of make-up	kmol/h
$HR_{\text{CaL}}$	CaL process heat ratio or heat distribution	-
$k$	deactivation constant	-
LHV	lower heating value	MJ/kg
$N$	number of cycles	-
$O_{2,\text{spec}}$	specific O <sub>2</sub> consumption	kgO <sub>2</sub> /kgCO <sub>2,capt</sub>
$p$	pressure	bar, bar(a), Pa
$P$	power	MW
$p_{\text{eq,CO}_2}$	equilibrium partial pressure	Pa
$p_{\infty}$	atmospheric pressure	Pa
$\dot{Q}$	heat flow	MW
$Q_{\text{f}}$	fuel heat input	MW
$Q_{\text{fuel}}$	specific fuel consumption	MJ/kgCO <sub>2,capt</sub>
$q_m$	mass flow rate	kg/s, t/a

$T$	temperature	°C, K
$T^*$	absolute temperature	K
$U_{mb}$	minimum bubbling velocity	m/s
$U_{mf}$	minimum fluidization velocity	m/s
$\dot{V}$	volumetric flow	Nm <sup>3</sup> /h
$x$	mass concentration	wt.%
$X_N$	sorbent carrying capacity	-
$X_r$	residual conversion capacity	-
$y$	volumetric concentration	vol.%

#### Greek characters

$\Delta H$	heat of reaction	kJ/mol
$\eta$	efficiency	%
$\lambda$	make-up ratio	-
$\Phi$	solid circulation ratio	-

#### Subscripts

abs	absorbed
ar	as received
CaL	calcium looping
calc	calciner
capt	captured
carb	carbonator
CO <sub>2</sub>	carbon dioxide

dh	district heat
dry	dry basis
e	electrical
eq	equilibrium
fan	fan
fuel	fuel
in	inlet
out	outlet
RC	recirculation
th	heat
tot	total
WtE	Waste-to-Energy plant

#### Abbreviations

APC	Air pollution control
ASU	Air separation unit
BA	Bottom ash
BECCS	Bioenergy carbon capture and storage
BFB	Bubbling fluidized bed
CaL	calcium looping
CCS	Carbon capture and storage
CCUS	Carbon capture, utilization, and storage
CFB	Circulating fluidized bed
CHP	Combined heat and power

CLC	Chemical looping combustion
COP21	United Nations Climate Conference in 2015
CPU	CO <sub>2</sub> compression and purification unit
EfW	Energy-from-Waste
FB	Fluidized bed
FG	Flue gas
GF	Grate-firing
GHG	Greenhouse gas
GPU	Gas processing unit
HRSG	Heat recovery steam generator
IGCC	Integrated gasification combined cycle
MEA	Monoethanolamine
MSW	Municipal solid waste
PSD	Particle size distribution
RDF	Refuse-derived fuel
SCR	Selective catalytic reduction
SNCR	Selective non-catalytic reduction
SRF	Solid recovered fuel
TRL	Technology readiness level
VOC	Volatile organic compound
WtE	Waste-to-Energy

## Table of contents

Abstract

Tiivistelmä

Acknowledgements

Symbols and abbreviations

1	Introduction .....	11
1.1	Structure of the Thesis .....	13
2	Waste-to-Energy.....	15
2.1	Classification of Wastes .....	16
2.2	Firing Concepts for Waste Fuels.....	18
2.3	Components of a Waste-to-Energy Plant.....	21
3	Carbon Capture.....	23
3.1	Pre-combustion .....	23
3.2	Post-combustion.....	24
3.3	Oxy-fuel Combustion.....	25
3.4	Chemical Looping Combustion .....	26
4	Calcium Looping .....	28
4.1	Process Concept .....	28
4.2	Fluidized Beds.....	34
4.3	Loss and Deactivation of Sorbent .....	36
4.4	Process Performance Indicators .....	40
5	Carbon Capture from Waste-to-Energy Plants.....	43
5.1	Current State of Carbon Capture from Waste-to-Energy Plants.....	43
5.2	Calcium Looping Implemented into Waste-to-Energy Plants .....	44
6	Modeling of Calcium Looping Process in Aspen Plus.....	49
6.1	Description of the Host Waste-to-Energy Plant.....	49
6.2	Basis for Modeling of the Calcium Looping Process .....	51
6.3	Model Description.....	51

6.4	Results and Discussion.....	57
6.4.1	Mass Balances.....	58
6.4.2	Power Production of the Calcium Looping Process .....	60
6.4.3	CO <sub>2</sub> Capture.....	64
6.4.4	Results Comparison to Other Studies .....	66
6.5	Further Development of the Model.....	68
7	Summary.....	70
	References.....	72

## Appendices

Appendix 1. Initial values and assumption for the simulation

Appendix 2. Stream results for main solid and gas flows

Appendix 3. Stream results for CO<sub>2</sub> capture

# 1 Introduction

It is scientifically evident that human activities have caused global warming, with the global surface temperature reaching 1.1°C above the pre-industrial levels (1850–1900) in 2011–2020 (IPCC, 2023). The rate of increase in global surface temperature for the 50-year period starting in 1970 is faster than any other 50-year period in at least the last 2000 years. The global warming is principally due to greenhouse gas (GHG) emissions that are dominated by the fossil CO<sub>2</sub> emissions. The concentration of CO<sub>2</sub> in the atmosphere reached its peak in 2019, exceeding the levels not seen at least in the past 2 million years with a concentration of 410 ppm. The effects of global warming are already observed around the globe. Sudden events such as extreme weather, drought, and floods have been observed as well as slow onset impacts such as higher temperatures, rainfall variability, glacier melting, sea level rise, and changes in disease distribution. The global mean sea level has increased by 0.20 m between 1901 and 2018. The sectors that are identified to be especially vulnerable to climate hazards are water, agriculture, ecosystems, health, and forestry. Global warming affects people's daily lives and economies. (IPCC, 2023; UNCCS, 2019)

In the United Nations Climate Change Conference (COP21) in Paris 2015, 196 parties adopted the legally binding international treaty on climate change, the Paris Agreement. According to the Paris Agreement, the parties agreed to substantially reduce the GHG emissions to hold the global warming below 2°C above the pre-industrial levels, and preferably limit the warming further to 1.5°C. (UNFCCC, 2015)

Although actions are done globally to reduce GHG emissions, there is an immense emission gap between the emission reductions promised and the emission reductions needed to achieve the temperature limit of the Paris Agreement. Currently, the efforts in place can limit the temperature increase to 2.8°C over the twenty-first century. To limit global warming to 1.5°C, a 45% reduction in global annual GHG emissions is needed from current emissions by 2030. (UNEP, 2022)

Energy-related GHG emissions have played a great role in the increasing GHG concentration in the atmosphere (Fawzy *et al.*, 2020). In 2022, the global energy-related GHG emissions were 41.3 Gt CO<sub>2</sub>-eq from the total GHG emissions of 53.8 Gt CO<sub>2</sub>-eq (Crippa *et al.*, 2023; IEA, 2023a). Fossil CO<sub>2</sub> accounted for 71.6% of the total GHG emissions. Energy-related

GHG emissions must be massively reduced to keep the world from warming above 1.5°C. For the energy production sector, the climate change mitigation approach includes conventional decarbonization technologies such as the introduction of renewable energy, nuclear power, improvements in energy efficiency, and carbon capture and storage. A newer mitigation approach is to implement negative CO<sub>2</sub> emission technologies such as bioenergy with carbon capture and storage (BECCS). (Fawzy *et al.*, 2020)

A growing population and rising living standards increase the amount of created municipal solid waste (MSW) annually. The share of CO<sub>2</sub> emissions from waste treatment and disposal is remarkable, estimation of 1.6 Gt CO<sub>2</sub>-eq in 2016 which is approximately 5% of global emissions (Kaza *et al.*, 2018). Waste management plays a crucial role in CO<sub>2</sub> emission reduction and achieving the goals of the Paris Agreement. Waste incineration is proposed as one of the best options for reducing the volume of waste and it serves as a possibility for energy recovery from the waste (Waste-to-Energy, or WtE) to answer the increasing energy needs of the growing population (Liu *et al.*, 2020). GHG emissions are reduced when waste incineration is used as an alternative to landfilling as methane emissions are eliminated which would otherwise be a significant emission from landfills. Using waste as an energy source instead of fossil fuels is also beneficial in GHG emission reduction due to the biogenic fraction that the waste contains. (Liu *et al.*, 2020)

Waste incineration creates CO<sub>2</sub> emissions. CO<sub>2</sub> emissions generated are estimated to be approximately 0.7–1.7 tonnes of CO<sub>2</sub> per tonne of MSW incinerated (Environment Agency, 2020). Typically, it is assumed that the biogenic fraction of MSW is 50%, but the ratio between fossil and biogenic carbon emissions is case-specific as it highly depends on the origin of the waste.

Conventional climate change mitigation efforts alone – reducing fossil CO<sub>2</sub> emissions – are not enough to limit global warming to the targets set in the Paris Agreement. It is evident that negative CO<sub>2</sub> emission technologies are needed to limit global warming to 2°C or further to 1.5°C (Gasser *et al.*, 2015). There is potential to reduce the fossil CO<sub>2</sub> emissions of waste incineration to zero or even create negative CO<sub>2</sub> emissions because of the biogenic carbon fraction present in the waste when implementing carbon capture and storage (CCS) processes in a Waste-to-Energy plant. Therefore, energy production with WtE implemented with CCS (WtE+CCS) provides an opportunity to generate energy with negative CO<sub>2</sub>

emissions, thus aiding in mitigating climate change with negative emission technology. (Kearns, 2019; Magnanelli *et al.*, 2021)

Calcium looping (CaL) represents a suitable option for post-combustion carbon capture from Waste-to-Energy plants as it may be retrofitted with relatively minor modifications to the host Waste-to-Energy plant or implemented to a newly built plant. The energy penalty of the CaL has been lower in the studies, compared to other post-combustion carbon capture processes. The CaL is based on the solid looping cycle. Limestone-based sorbents which are easily available with low cost, are used to capture CO<sub>2</sub> from the flue gases (FG) of the large CO<sub>2</sub> point source. (Yang *et al.*, 2010) Carbon capture is achieved as the sorbent goes through cyclic carbonation – calcination reactions in the two interconnected circulating fluidized bed (CFB) reactors, called carbonator and calciner. A supplementary fuel is combusted in the calciner to provide the required heat for the process. CaL has been successfully demonstrated on a megawatt-scale, with different fuels such as coal (Diego and Arias, 2020), and with conditions typical for a Waste-to-Energy plant applying waste-derived supplementary fuels in the calciner (Haaf, Hilz, *et al.*, 2020). However, there is still little research available in the literature on CaL application for the decarbonization of a WtE plant.

This thesis aims to investigate a tail-end CaL application for the decarbonization of a WtE plant via a literature review and simulations in Aspen Plus. The main objectives are to evaluate the heat and mass balances of the tail-end CaL system, evaluate how the tail-end CaL system implemented to a WtE plant affects the CO<sub>2</sub> balance of the WtE plant and what is the impact of different fuels combusted in the calciner to the CaL system performance. Via literature review, the energy penalty of the CaL process and the heat integration opportunities are discussed.

## 1.1 Structure of the Thesis

The literature review of the thesis consists of four parts: Chapter 2 Waste-to-Energy, Chapter 3 Carbon Capture, Chapter 4 Calcium Looping, and Chapter 5 Carbon Capture from Waste-to-Energy Plants.

In Chapter 2 an introduction to waste incineration is given. The classification of waste is discussed, alternative firing concepts for waste firing, and the typical components of a waste-to-energy plant are introduced.

Chapter 3 reviews different carbon capture concepts, including pre-combustion, post-combustion, and oxy-fuel combustion.

Calcium looping is discussed more in detail in Chapter 4. Here, the process concept is described and an introduction to fluidization is given as in this work CFB reactors are applied to the CaL process. The mechanisms that affect the circulating sorbent in the CaL process are introduced together with main process performance indicators.

Chapter 5 discusses the current state of carbon capture from WtE plants and presents the heat integration options between CaL system and WtE plant. The energy penalty of the CaL process is also discussed.

The practical part of this thesis is covered in Chapter 6 Modeling of Calcium Looping Process in Aspen Plus. The simulation model created in Aspen Plus is described and the results obtained from the simulation are presented and discussed.

In Chapter 7 Summary, the outcome of the thesis is summarized.

## 2 Waste-to-Energy

Waste incineration has the objective to reduce the volume and hazardousness of waste, such as municipal solid waste (MSW), by burning it in a combustion chamber. Recovering of energy from MSW and other waste streams has become an important second objective for waste incineration. This concept is then called Waste-to-Energy (WtE) or Energy-from-Waste (EfW). (Neuwahl, Frederik *et al.*, 2019) Waste incineration presents one conversion technique in the thermo-chemical conversion route. Besides incineration, gasification and pyrolysis represent a thermo-chemical route to convert waste to energy. The thermo-chemical conversion process is illustrated in Figure 1. (Leckner, 2015)

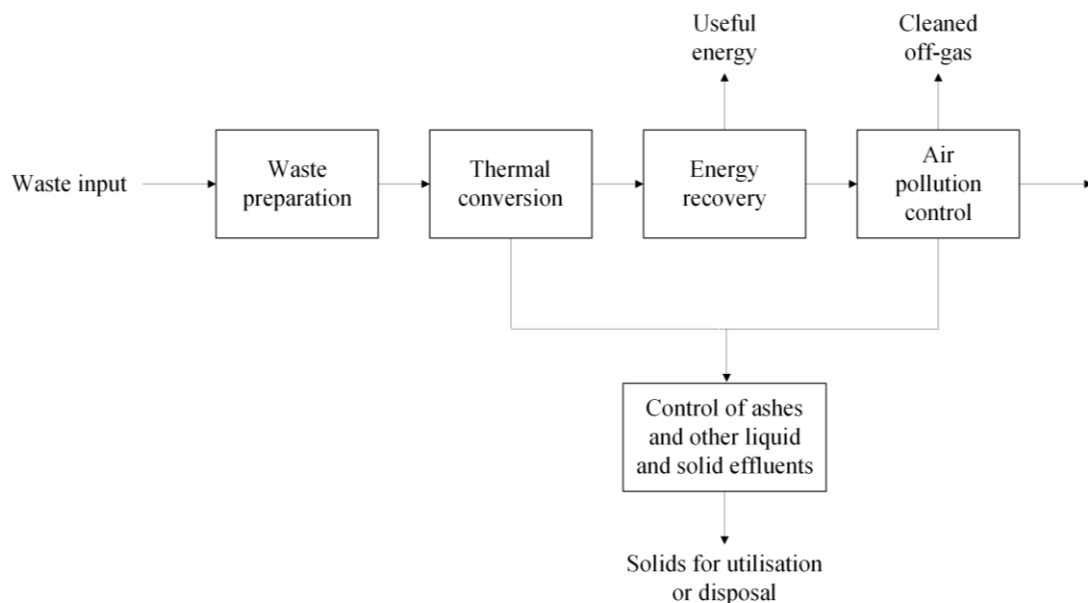


Figure 1. A waste to energy system based on thermal conversion. Adapted from (Leckner, 2015), re-created for clarity.

The thermal conversion process of waste includes two main steps: Waste preparation and the application of heat to convert it into usable energy. Before converting waste into usable energy with the application of heat, waste is sorted and pre-treated according to the needs of the used thermal conversion technique. Pre-treatment processes include mixing and homogenization, shredding, and sorting out heavy materials and metals. (Leckner, 2015)

In this chapter, the types of waste for incineration are introduced. A brief overview to the most common firing concepts for MSW is provided and lastly, the main components of a WtE plant are discussed.

## 2.1 Classification of Wastes

Waste can be classified based on the origin of the waste (e.g., from households or industrial), its nature (e.g., hazardous) or the method used for its management (e.g., collected separately). The main types of wastes that are incinerated are untreated MSW, pre-treated municipal wastes, such as refuse-derived fuel (RDF) or solid recovered fuel (SRF), non-hazardous industrial wastes and packaging, hazardous wastes, sewage sludges, and clinical wastes. (Neuwahl, Frederik *et al.*, 2019)

Waste fuels contain fractions of both biomass and fossil origin. Biomass means material that has an organic origin. Determining the biomass content of the waste fuel is important so that the impact on GHG emissions can be evaluated when waste fuel is used in energy production. Carbon emissions resulting from biomass combustion are biogenic. This means that CO<sub>2</sub> emissions from biomass are considered carbon neutral, because while growing, biomass sequesters carbon and during combustion, it is released back to the carbon cycle. Therefore, CO<sub>2</sub> emissions from the combustion of waste fuels are partly biogenic. (IEA Bioenergy, 2023; SFS-EN ISO 21644:2021:en, 2021)

The composition of MSW varies depending on the source. Higher-income countries tend to generate more waste than lower-income countries, but the organic portion of the waste is decreased with increasing income levels (Kaza *et al.*, 2018). According to Global CCS Institute (2019), the typical distribution between biogenic and fossil carbon is 42% and 58%, respectively. It is though often seen that the biogenic fraction of MSW is assumed to be 50% in the literature. In Figure 2 the amounts of biogenic and fossil carbon in MSW incinerated in a WtE plant as well as the generated amount of biogenic vs. fossil carbon dioxide emissions are seen.

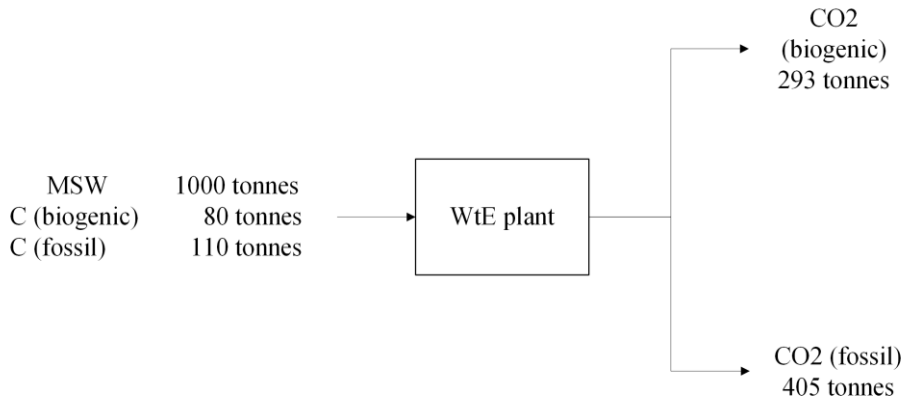


Figure 2. The amount of biogenic and fossil carbon in MSW, and the generated biogenic and fossil carbon dioxide emissions. Modified from (Kearns, 2019)

### Solid Recovered Fuel

SRF is derived from non-hazardous MSW or industrial waste and can contain for example plastics, wood, cardboard, paper, or textiles. Untreated MSW as such cannot be considered as SRF. Standardization for waste fuels exists and one such standard is SFS-EN ISO 21640:2021, which classifies SRF. The standard defines the acceptable material flows for SRF production that are not suitable for recycling. The materials can originate from industry, construction and demolition, waste-management facilities, material recycling facilities, municipalities, or commercial sources. The limit values in the SRF classification system are the lower heating value (LHV) and the contents of chlorine and mercury. Also, other properties such as particle size and moisture content are mandatory to be specified. (SFS-EN ISO 21640:2021:en, 2021)

The biomass content is not mandatory to specify though needed to calculate the emission of biomass or fossil carbon dioxide per unit of SRF. Biomass content can be determined according to ISO 21644 standard. (SFS-EN ISO 21640:2021:en, 2021)

Refuse-Derived Fuel (RDF) is similar to SRF, also derived from non-hazardous waste streams, but the classification of RDF doesn't follow standardized procedures as in the production of SRF. Therefore the quality is not as proven as SRF's. (Velis *et al.*, 2010)

## 2.2 Firing Concepts for Waste Fuels

Grate-firing (GF), fluidized bed (FB), and rotary furnace (or rotary kiln) are the firing devices in use for MSW conversion. GF is the traditional system that has been in use the longest for waste incineration, while FB has been in use for waste incineration for a shorter time. Rotary furnaces are mainly in use for incineration of hazardous and other special waste types. In this work, GF and FB devices are briefly introduced to provide an introduction to the most common MSW firing concepts. (Leckner and Lind, 2020)

### Grate-Firing

In GF (also called mass burning) the waste fuel is burned on a grate that is typically inclined horizontally approximately  $10\text{-}25^\circ$ . The fuel is fed through the feed chute to the fuel shaft where the fuel feed mechanism presses the fuel from the fuel shaft onto the grate. The size of the fuel can be anything that passes the fuel feed chute. A fuel feeder may be a hydraulic ramp or other type of conveying system. In Figure 3, a principle of a GF boiler is presented. (Leckner and Lind, 2020; Neuwahl, Frederik *et al.*, 2019)

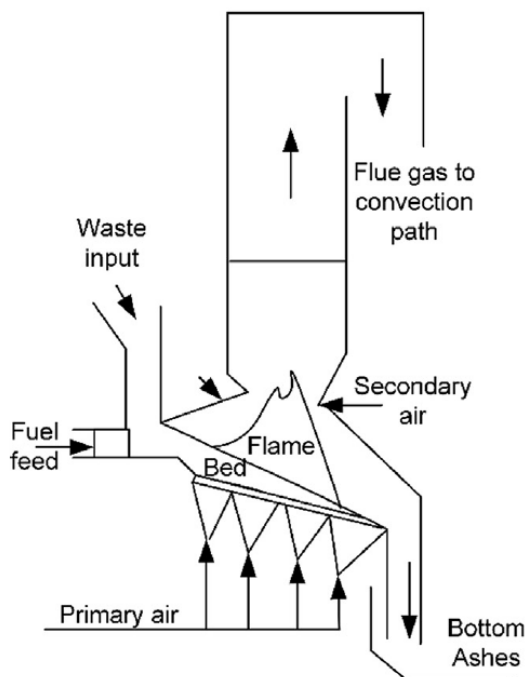


Figure 3. Principle of a GF boiler. (Leckner and Lind, 2020)

The fuel is incinerated on the grate. The grate stirs and looses the fuel material and transports it along the grate. The residence time of the waste fuel on the grate is usually approximately 60 minutes. The grate consists of rods that move in forward or reverse motion. Primary combustion air is fed from beneath through the grate into the furnace in several sections to provide air needed for all the stages of conversion: drying, devolatilization, combustion of gases, and char combustion. Secondary combustion air is generally added above the waste bed to achieve complete combustion. (Leckner and Lind, 2020; Neuwahl, Frederik *et al.*, 2019)

While the fuel bed moves forward along the grate, the reaction front develops and moves downwards in the bed simultaneously. Clear distinction of conversion zones may not be detected because of the stirring of fuel, caused by the movement of rods, which also correspondingly blurs the conversion zones. Initially, the thickness of the fuel layer on the grate is approximately one meter. The length of the grate is determined based on the needed length for burnout of the char, typically the length of the grate is approximately 10 m. Parallel grate modules are added side by side to adapt to the fuel power. (Leckner and Lind, 2020)

The bottom ash (BA) is discharged from the end of the grate to the BA discharger which also acts as an air seal for the furnace. It prevents FG emissions and uncontrolled air ingress to the furnace. The BA discharger cools down the ash. (Neuwahl, Frederik *et al.*, 2019)

### **Fluidized Beds**

Two types of FB boilers are used for MSW incineration: circulating fluidized bed (CFB) and bubbling fluidized bed (BFB). BFBs are used in smaller scale, plants that have a fuel feed less than 10 t/h. In Figure 4 the principle of both of the FBs are shown. (Leckner and Lind, 2020)

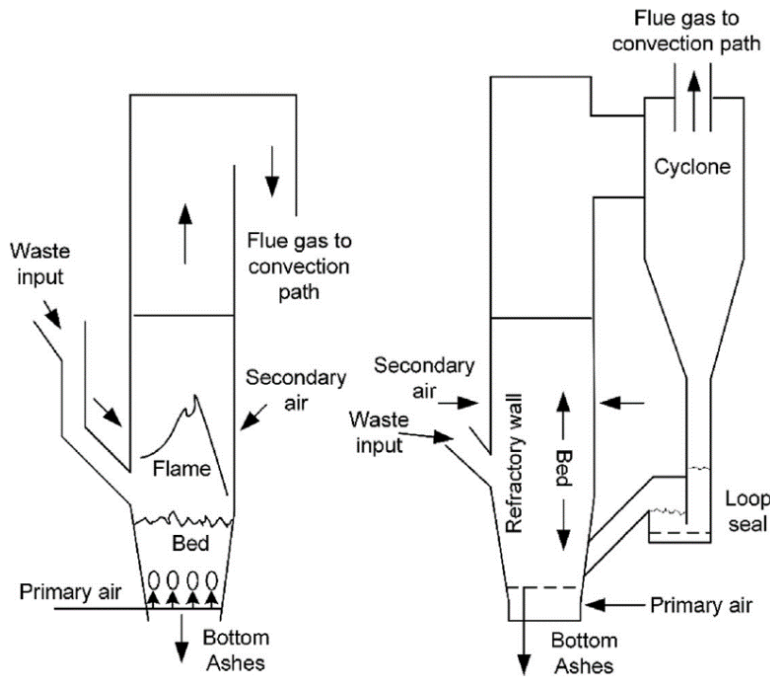


Figure 4. Principle of BFB (left) and CFB (right) for waste incineration. (Leckner and Lind, 2020)

Waste fuel is combusted in a bed of inert material, such as silica sand or ash. An FB combustor is typically a vertical combustion chamber. Waste is fed to the lower section into the bed of inert particles. The height of the bed without fuel before fluidization is approximately one meter. The bed is fluidized by preheated primary combustion air that enters the chamber from the bottom. Secondary air may be injected at a higher level in the chamber. In BFBs, drying, volatilization, ignition, and combustion take place in the bed and the volatiles burn in the free space above the bed. The free space allows an adequate residence time for the gases in the combustion zone. In CFBs, the conversion occurs in the entire reactor, but it is the greatest in the bottom. The combustion of waste requires  $850^{\circ}\text{C}$ . (Leckner and Lind, 2020; Neuwahl, Frederik *et al.*, 2019)

The advantage of FB incineration is good mixing in the reactor which leads to uniform temperature and oxygen concentration. These assist the stable operation of the reactor. The bed has a large thermal inertia, which means it acts as a “thermal flywheel” capable of withstanding short-term variations in fuel quality and supply (Leckner and Lind, 2020). The particle size of the fuel should be rather small with a maximum diameter of 50 mm for FB incineration. Heterogeneous waste is pre-treated according to size specifications by sorting, crushing, and shredding. (Neuwahl, Frederik *et al.*, 2019)

### 2.3 Components of a Waste-to-Energy Plant

At first waste incineration only served the purpose of reducing the amount of waste by burning it to ashes. Now, the energy recovery from the heat of combustion is implemented and the facilities have become WtE plants. Traditionally, there has been a distinction between the incinerator and the boiler, which contains the heat transfer surfaces for steam production. As the current waste incineration plants also include energy recovery, the concept of waste incineration is closer to combustion and the incinerator device is closer to the boiler in a general sense. The components of a WtE plant can be subdivided as seen in Figure 5. (Leckner and Lind, 2020)

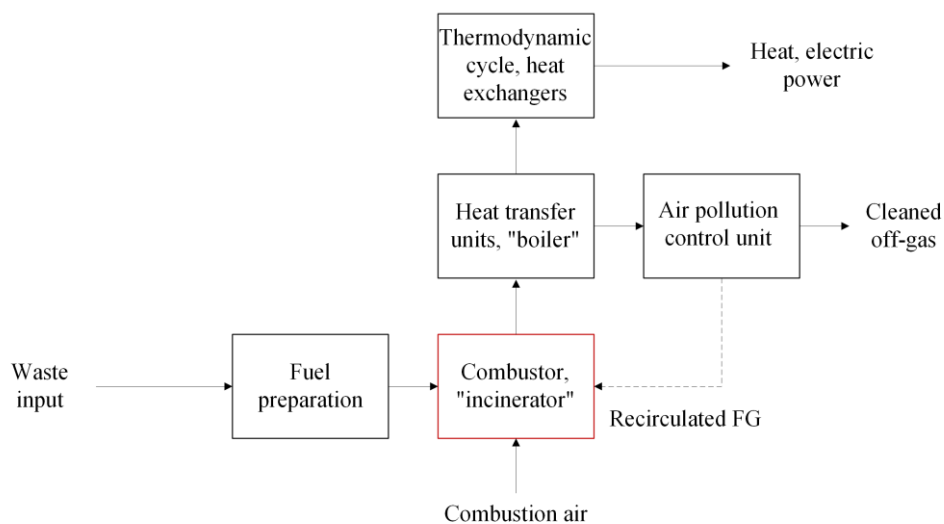


Figure 5. The subdivision of components in WtE plant. Adapted from (Leckner and Lind, 2020), re-created for clarity.

The combustor may be a GF unit, a FB, or a rotary kiln as discussed earlier in Chapter 2.2. Energy is recovered in the boiler to produce steam. In the thermodynamic cycle, the recovered energy is converted to electricity and heat for consumers. Air Pollution Control (APC) devices are needed to clean the FG to stay within the emission limits. (Leckner and Lind, 2020)

Emissions to air from the stack of a WtE plant are dust, acid gases,  $\text{NO}_x$ , heavy metals, such as mercury (Hg),  $\text{CO}_2$ , and other carbon compounds, for instance, CO and volatile organic

compounds (VOC). Individual process units designed to remove specific pollutants from the FG are combined together to form the complete FG cleaning system. (Neuwahl, Frederik *et al.*, 2019; Shareefdeen and Mishu, 2021)

Bag filters are very widely used for reducing dust emissions in waste incineration plants. An electrostatic precipitator is another option for reducing dust emissions. The system can also include both mentioned techniques. For the reduction of acid gas emissions, wet processes, semi-wet processes, and dry processes are applied. The techniques are based on the injection of alkaline reagents which are brought into contact with the FG. The reaction products are dissolved or dry salts. Only wet processes have dissolved salts as a product, otherwise, the products are dry salts. Wet processes include the use of a scrubber, for example, jet scrubber or spray scrubber. Semi-wet processes are combined with a bag filter. (Neuwahl, Frederik *et al.*, 2019; Shareefdeen and Mishu, 2021)

For the reduction of NO<sub>x</sub> emissions, primary techniques and secondary techniques may be applied. Primary techniques include measures for furnace control, such as preventing oversupply of air or using unnecessarily high furnace temperatures. Typically, primary techniques alone are not enough, therefore, secondary techniques are needed to meet the NO<sub>x</sub> emission limits. The most important processes used are selective non-catalytic reduction (SNCR) and selective catalytic reduction (SCR). Both processes include the application of ammonia or urea as a reduction agent. In SNCR, ammonia is injected into the furnace where it reacts with NO<sub>x</sub> and produces nitrogen and water. In SCR, an ammonia-air mixture is added to the FG and passed over a catalyst, where ammonia reacts with NO<sub>x</sub> to give nitrogen and water. (Neuwahl, Frederik *et al.*, 2019; Shareefdeen and Mishu, 2021)

### 3 Carbon Capture

Carbon capture, utilization, and storage (CCUS) is a promising technology for decarbonizing the power and carbon-intensive industry sectors. In CCUS technology the CO<sub>2</sub> is captured from large point sources that rely on fossil fuels such as coal, oil, or gas. The captured CO<sub>2</sub> is either utilized on-site or compressed and transported to be utilized elsewhere in different applications such as in the production of chemicals, fuels, or building materials, or stored in geological reservoirs. CCUS can also be applied to biogenic CO<sub>2</sub> sources; it then leads to negative CO<sub>2</sub> emissions. In that case, it is referred to as bioenergy with carbon capture and storage (BECCS). (Fawzy *et al.*, 2020; IEA, 2023b, 2023c)

The carbon capturing concepts for separating CO<sub>2</sub> from large point sources are pre-combustion, post-combustion, oxy-fuel combustion and chemical looping combustion. In the following sections, these CO<sub>2</sub> capture concepts will be introduced.

#### 3.1 Pre-combustion

Pre-combustion is a carbon capture concept to capture the CO<sub>2</sub> before the combustion process. It can be achieved through gasification of a fuel or steam reforming of a gas. In Figure 6 a pre-combustion carbon capture concept is outlined for both gasification path and steam reforming path.

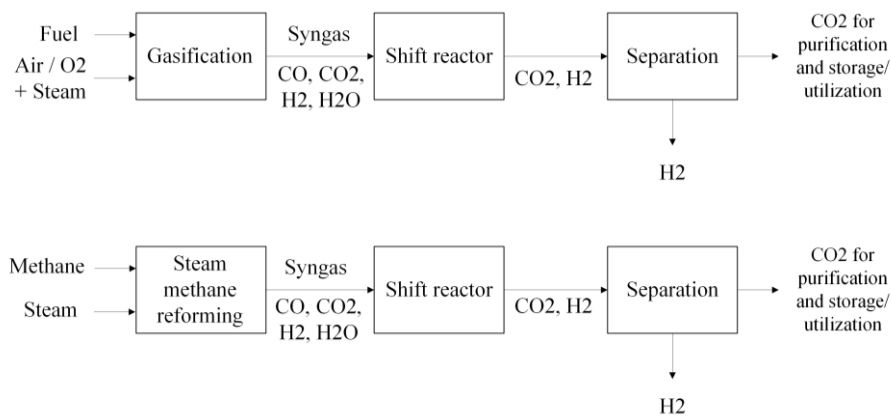


Figure 6. Pre-combustion carbon capture via gasification and steam methane reforming. Adapted from (IEAGHG, 2019), re-created for clarity.

Pre-combustion carbon capture consists of four major stages (Carpenter and Long, 2017):

1. Firstly, the fuel is converted into syngas via gasification or steam methane reforming. Syngas consists mainly of CO and H<sub>2</sub>.
2. The syngas is led to a shift reactor, where CO reacts with water. This is the water-gas shift reaction. The products of the reaction are CO<sub>2</sub> and H<sub>2</sub>.
3. CO<sub>2</sub> is separated from H<sub>2</sub> using absorption by physical or chemical solvents, or adsorption by porous materials.
4. Lastly, CO<sub>2</sub> is liquefied, compressed, and bottled for further use, or stored.

The pre-combustion carbon capture concept is especially an attractive solution for carbon capture within the Integrated Gasification Combined Cycle (IGCC). The syngas produced in IGCC has typically relatively high partial pressure of CO<sub>2</sub>. The possibility to separate CO<sub>2</sub> from the syngas in above ambient pressures reduces the required energy for compression of CO<sub>2</sub>. (IEAGHG, 2019)

### 3.2 Post-combustion

In a post-combustion carbon capture concept, the CO<sub>2</sub> is removed from the FG stream after the combustion process (IEAGHG, 2019). It is applicable to industrial plants, such as steel or cement plants or power plants. Post-combustion concept represents the most suitable option for retrofitting existing plants because only relatively minor modifications need to be made to the host plant. The post-combustion process is presented in Figure 7. (Nanda *et al.*, 2022, pp. 4–9)

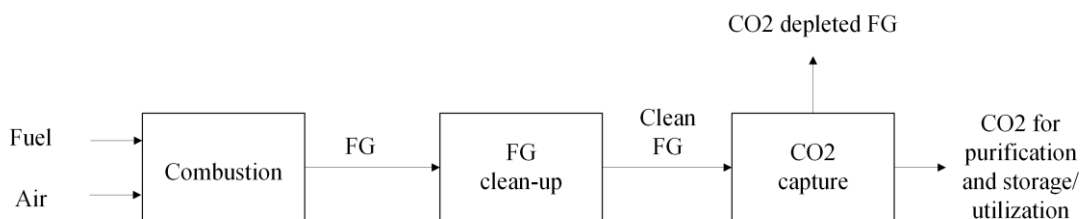


Figure 7. Post-combustion process. Adapted from (IEAGHG, 2019), re-created for clarity.

Exhaust gases are cleaned from particulate matter, nitrogen oxides ( $\text{NO}_x$ ), and sulfur oxides ( $\text{SO}_x$ ) and are then fed to the  $\text{CO}_2$  capturing process. Post-combustion carbon capture can be based on chemical absorbents, absorption to solids such as  $\text{CaO}$ , or membrane separation for instance. The most typical absorbents are an amine-based solvent such as monoethanolamine (MEA), which has become the benchmark amine for  $\text{CO}_2$  capture from electricity production due to its technological maturity and suitability to low  $\text{CO}_2$  partial pressure applications. Other solvents can also be used that are not amine-based such as alkaline solutions  $\text{KOH}$  and  $\text{NaOH}$ . (Bui *et al.*, 2018)

MEA is the most extensively developed process among all carbon capture processes and it is already applied in commercial scale (Bui *et al.*, 2018). The first post-combustion carbon capture based on MEA was applied commercially in Boundary Dam coal-power plant in Canada (SaskPower, 2023). Petra Nova in Texas is another commercially operating post-combustion carbon capture process based on MEA (U.S Department of Energy, 2017). CaL is considered as a post-combustion carbon capture technique. It will be further discussed in Chapter 4.

### 3.3 Oxy-fuel Combustion

An oxy-fuel combustion process involves separation of oxygen from air and combusting fuel in the absence of nitrogen. As a product from oxy-fuel combustion, a relatively pure  $\text{CO}_2$  stream is produced. In Figure 8 an oxy-fuel combustion process is shown.

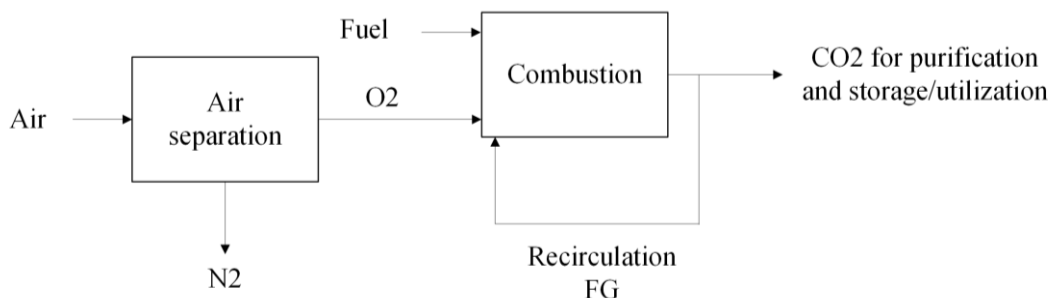


Figure 8. Oxy-fuel combustion process. Modified from (IEAGHG, 2019).

Nitrogen is removed from the air in an air separation unit (ASU) prior to combustion. Typically, the oxygen delivered by the ASU has a purity of 95-97 % (IEAGHG, 2019). Combusting fuel in high-purity oxygen produces FG that contains mainly CO<sub>2</sub> and H<sub>2</sub>O. Burning fuel in pure oxygen causes the flame temperature to rise excessively high. Therefore, the oxygen stream must be diluted with an inert stream to control the flame temperature. The ways to carry out the dilution of the combustion oxygen are recirculation of the FG or steam injection. (Leckner, 2023)

### 3.4 Chemical Looping Combustion

In chemical looping combustion (CLC) the fuel is combusted in the presence of oxygen as well as in the oxy-fuel combustion process, but the oxygen is provided to the combustion chamber by a solid oxygen carrier that is usually metal-based. In CLC no ASU is needed and therefore there is no energy penalty related to the operation of the ASU compared to the conventional oxy-fuel combustion process. (Di Giuliano *et al.*, 2022)

Typically, the CLC system is composed of two interconnected FB reactors. Air and metal particles are fed to the air reactor to oxidize the metal. Metal oxides act as an oxygen carrier between the reactors. The fuel is combusted in the fuel reactor by the reduction of the oxygen carrier. Reduced metal oxides are then fed back to the air reactor. This way oxygen carrier particles form a loop while circulating between the reactors. In Figure 9 a CLC system using FBs reactors is presented. (Di Giuliano *et al.*, 2022)

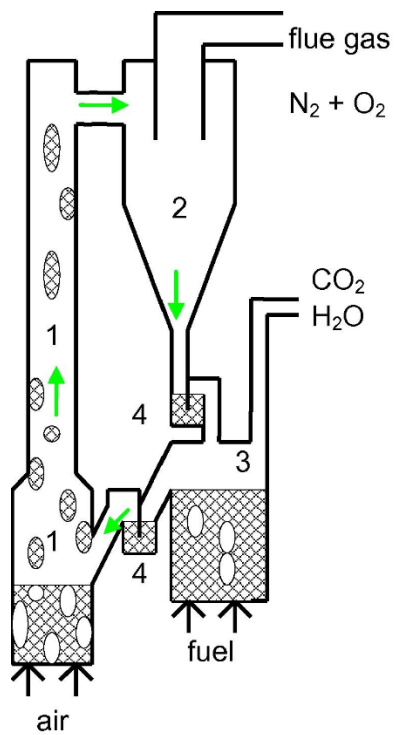


Figure 9. CLC system with interconnected fluidized bed reactors (Lyngfelt, 2014)

In the CLC system presented above, the metal oxides from the air reactor and riser (1) are separated from depleted air in a cyclone (2) before being fed to the fuel reactor (3) through a loop seal (4). Fluidization gases are isolated within the reactors by the loop seals. The FG that is formed during combustion mainly consists of CO<sub>2</sub> and H<sub>2</sub>O. CO<sub>2</sub> may be separated for utilization or storage.

## 4 Calcium Looping

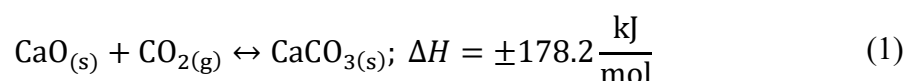
Calcium looping (or carbonate looping, CaL) is a second-generation post-combustion (see Chapter 3) carbon capture technology. It was first introduced in 1999 for capturing CO<sub>2</sub> from coal-fired power plants by Shimizu *et al.* (1999). CaL may be retrofitted to power plants or industrial processes, such as the cement process. As a post-combustion technology, a CaL retrofit requires only minor modifications to the host plant. Additionally, when retrofitting CaL into cement plants, positive synergies arise from the fact that both processes utilize natural limestone. Therefore, the spent sorbent material from CaL can potentially be used in the cement host process. (Atsonios *et al.*, 2015)

CaL is currently at a technology readiness level (TRL) of 7 (European Commission, 2021). That means that the technology has been demonstrated in an operational environment. For comparison, post-combustion carbon capture based on MEA is at TRL of 9, which means that the technology has been proven in its operational environment and commercialized (See Chapter 3.2). (Raffaini and Manfredi, 2022)

In this chapter the concept of CaL is discussed including the functional description of carbonator and calciner. An introduction to fluidized beds and fluidization will be given. The topic of sorbent loss and deactivation is introduced. At the end of the chapter the main CaL process performance indicators are introduced.

### 4.1 Process Concept

The CaL process relies on the reversible carbonation-calcination reaction of calcium oxide (CaO) that is used as a sorbent in a solid circulation system. (Shimizu *et al.*, 1999) The carbonation-calcination reaction of limestone is expressed in Equation (1). Heat is released when calcium carbonate (CaCO<sub>3</sub>) is formed via the carbonation of CaO and correspondingly heat is required to regenerate CaCO<sub>3</sub> into CaO via calcination.



The chemical equilibrium conditions between carbonation and calcination controls the characteristics of the CaL process. The equilibrium concentration of CO<sub>2</sub> is dependent on the prevailing temperature in the process. The equilibrium curve for carbonation-calcination may be plotted based on Equation (2) proposed by Silcox et al. (1989):

$$\frac{p_{\text{eq,CO}_2}}{p_{\infty}} = 4,137 \times 10^7 \times e^{\frac{-20474 \text{ K}}{T^*}} \quad (2)$$

Where  $p_{\text{eq,CO}_2}$  is the equilibrium partial pressure of carbon dioxide [Pa],  $p_{\infty}$  is atmospheric pressure and  $T^*$  represents the absolute temperature [K]. In Figure 10 the chemical equilibrium curve resulting from Equation (2) is shown.

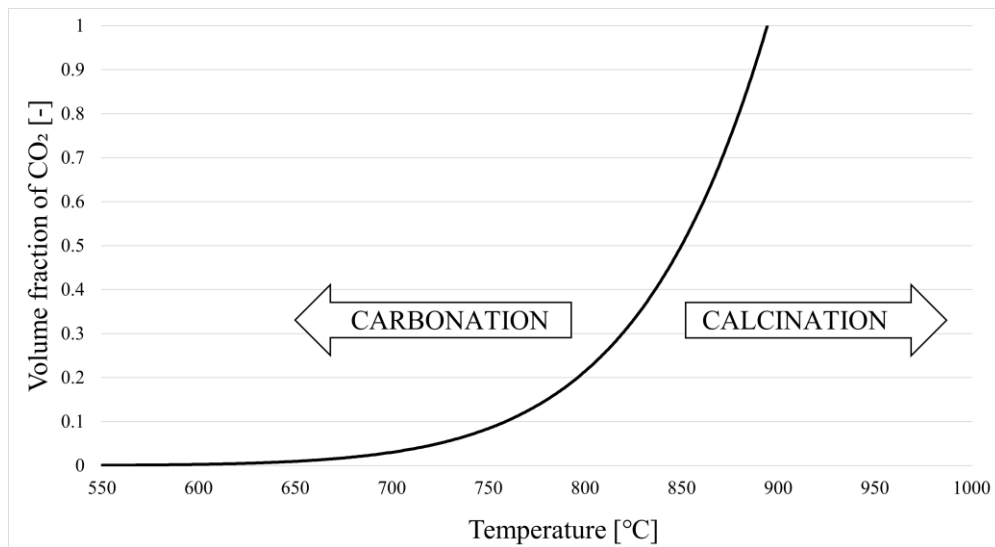


Figure 10. The chemical equilibrium curve between carbonation and calcination reaction

A CaL system consists of two interconnected reactors, a carbonator and a calciner. CO<sub>2</sub> is captured in the first reactor, the carbonator, in a forward reaction according to Equation (1). The carbonator is operated at approximately 650°C. A CO<sub>2</sub>-rich stream is released from the calciner, also called a regenerator, after the endothermic reaction. The heat required for endothermic calcination reaction is provided by burning fuel in the calciner in an oxy-fuel atmosphere. The oxy-fuel combustion enables the production of a relatively pure CO<sub>2</sub> stream

as it is not diluted with nitrogen as in air combustion (Leckner and Gómez-Barea, 2014). The combustion oxygen is diluted with recirculated FG to control the burning rate. Regeneration of the sorbent in the calciner takes place at approximately 900°C (Martínez *et al.*, 2012). In Figure 11, a schematic of the CaL process is presented.

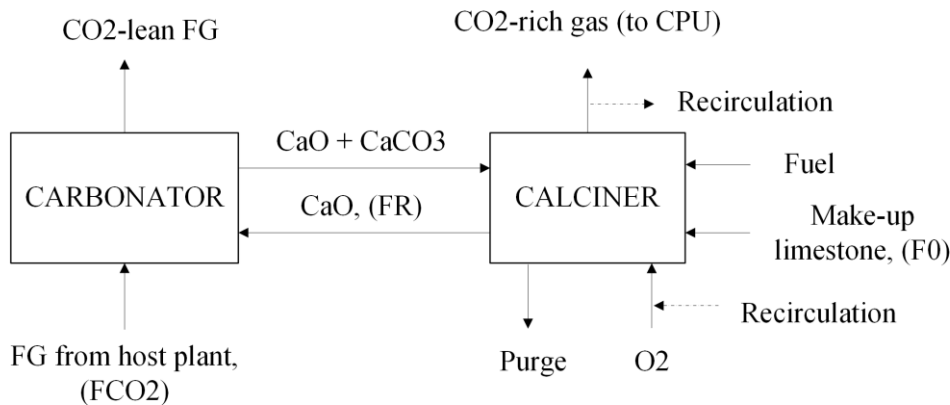


Figure 11. Schematic of the calcium looping process.

The main material streams that are commonly discussed in the literature when analyzing the characteristics of the CaL process are the molar flows within the system: the molar flow of CO<sub>2</sub> that is fed to the carbonator with the FG from the host plant,  $F_{CO_2}$ , the molar flow of Ca-species that circulates between the calciner and the carbonator,  $F_R$ , and the molar flow of fresh limestone in the make-up flow that is fed to the calciner to provide fresh sorbent to the system,  $F_0$ .

A cryogenic ASU provides the oxygen to the calciner. Also, oxygen as a by-product from electrolysis can be used as an oxygen source for the calciner (Hein *et al.*, 2013). The produced rich CO<sub>2</sub> gas is purified in the CO<sub>2</sub> compression and purification unit (CPU), also called the gas processing unit (GPU), before transportation, storage, and/or utilization. A solid purge flow is led out of the calciner, and fresh sorbent is fed to the calciner to make up the lost sorbent. The reasons for the need for the purge flow will be discussed in Chapter 4.3.

## Carbonator

The  $\text{CO}_2$  in the FG fed to the carbonator from the host plant reacts with the  $\text{CaO}$ , forms calcium carbonate ( $\text{CaCO}_3$ ), and heat is released according to Equation (1). An exemplary layout of a CFB type of carbonator reactor is presented in Figure 12. The carbonator also desulfurizes the FG if  $\text{SO}_2$  is present in the FG. Sulfation can happen in two possible ways according to Equations (3) and (4) (Jeong *et al.*, 2015). In the carbonator,  $\text{SO}_2$  capture efficiencies of 0.95 can be achieved according to Arias *et al.* (2013). (Arias *et al.*, 2013; Haaf, Anantharaman, *et al.*, 2020)

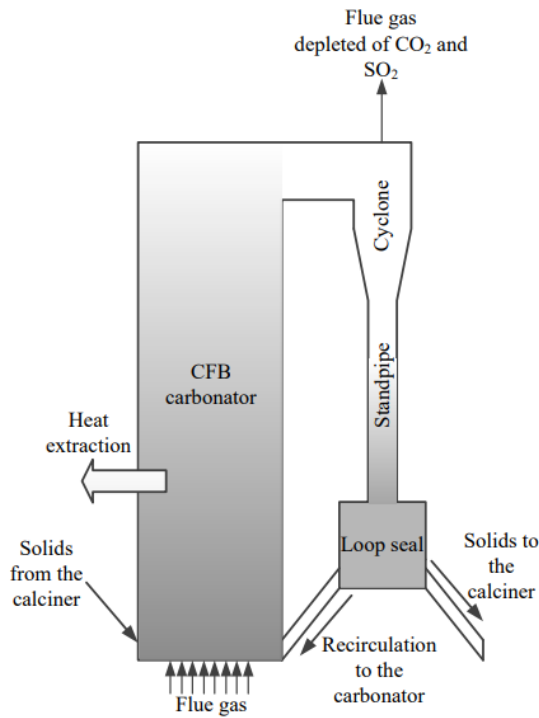
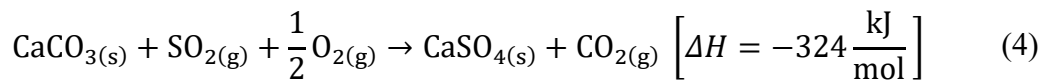
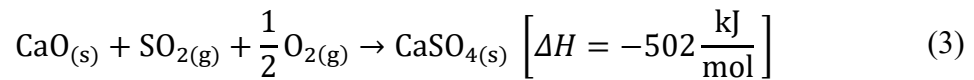


Figure 12. The layout of a CFB carbonator reactor. (Ylätalo, 2013)

The carbonator reactor is equipped with heat extraction devices because exothermic carbonation reaction releases heat and additional heat is brought to the carbonator by hot solids flowing from the calciner. The conditions in the carbonator are kept on the carbonation side of the chemical equilibrium curve seen in Figure 10. (Blamey *et al.*, 2010; Shimizu *et al.*, 1999)

The carbonation reaction occurs in two stages. In the beginning, the carbonation is rapid and is controlled by the chemical reaction kinetics (fast regime). When the thickness of the  $\text{CaCO}_3$  product layer covering the sorbent particle reaches the critical level of approximately 50 nm,  $\text{CO}_2$  can only react with  $\text{CaO}$  after diffusing through the layer and reaching the  $\text{CaO}$  surface. The carbonation reaction rate then slows down considerably because it is limited by the diffusion (slow regime). (Erans *et al.*, 2016) These different stages are presented in Figure 13.

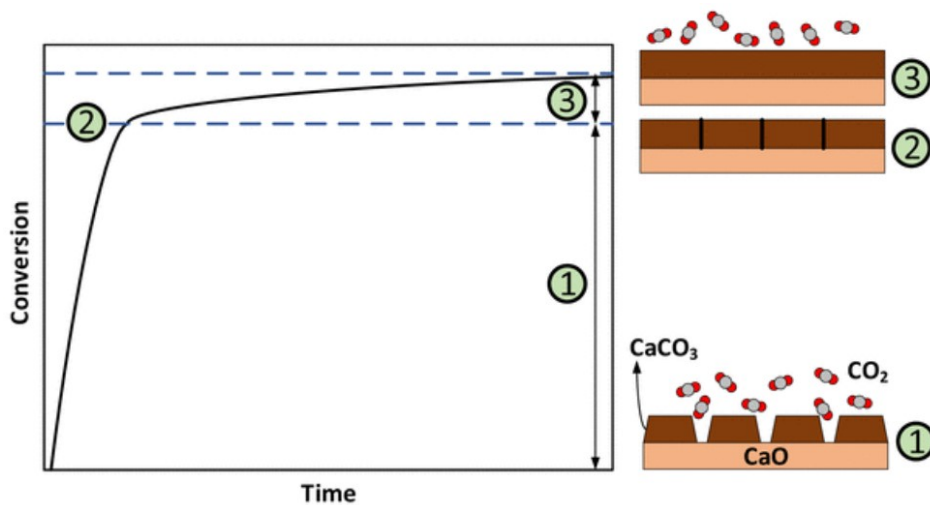


Figure 13. Carbonation stages (Nanda *et al.*, 2022, p. 166)

The conversion stages in the carbonation reaction are presented as a function of reaction time. A fast regime is indicated with a number (1) in the figure. The thickness of the  $\text{CaCO}_3$  product layer has reached the critical level at point (2). A slow regime of carbonation reaction occurs between the blue dashed lines (3).

## Calciner

$\text{CaCO}_3$  formed in the carbonator is transferred to the calciner. The heat required by the calcination reaction according to the reverse reaction of Equation (1) is provided by oxy-fuel combustion of supplementary fuel that is fed to the calciner. Sulfation may occur in the calciner according to Equations (3) and (4) due to  $\text{SO}_2$  introduced to the calciner by the supplementary fuel. An exemplary layout of a CFB calciner is represented in Figure 14.

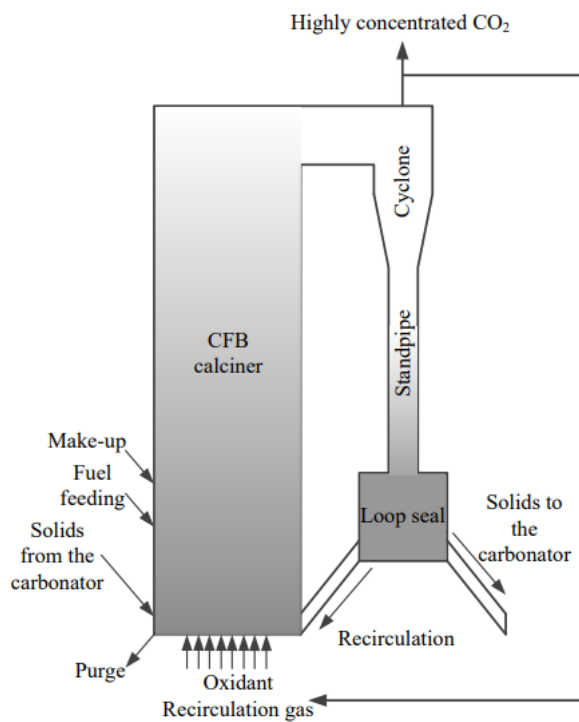


Figure 14. The layout of a CFB calciner. (Ylätaalo, 2013)

Higher temperatures in the calciner increase the calcination reaction rate but cause rapid degradation of the sorbent. Lower temperatures on the other hand enable the sorbent to degrade less but decrease the calcination reaction rate. Eventually, if the temperature is low enough the equilibrium conditions shift towards carbonation as seen in Figure 10 and the regeneration of the sorbent is prevented. (Dean *et al.*, 2011)

A constant solid purge flow out of the calciner is needed due to multiple reasons. In general, its purpose is to remove spent sorbent from the system as well as to remove inert species such as calcium sulfate ( $\text{CaSO}_4$ ) and ash that would otherwise accumulate in the system. The

deactivation and loss of sorbent are related to the need of constant purge flow and are discussed in Chapter 4.3. The fresh sorbent is fed to the calciner to maintain the desired CO<sub>2</sub> carrying capacity of the sorbent, so the ability of the sorbent to absorb CO<sub>2</sub> from the FG stream. (Erans *et al.*, 2016; Rodriguez *et al.*, 2008)

## 4.2 Fluidized Beds

A bed of solid particles is fluidized when gas is fed through the bed so that the particles are floating in an upward motion. Distinction in the behavior of fluidized solids can be detected as the superficial gas velocity through the bed of solid particles increases. With the change in the gas velocity, the bed moves from one regime of fluidization to another. (Basu, 2015) Regimes of fluidization are presented in Figure 15.

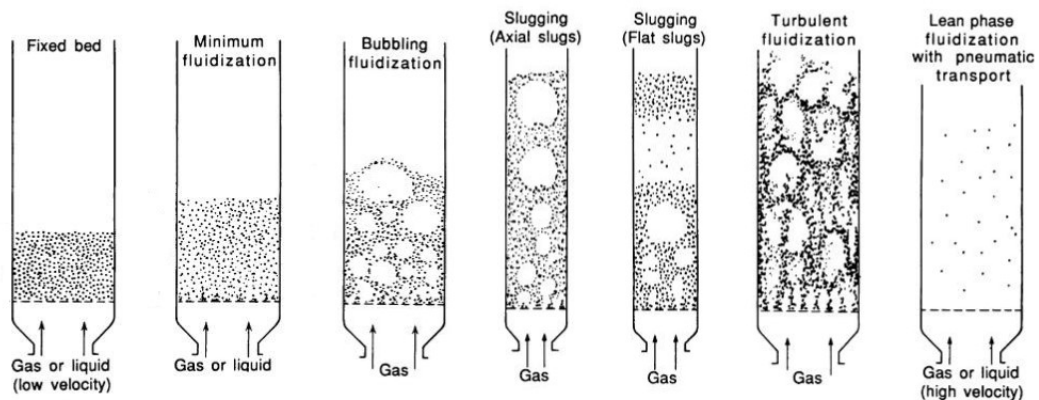


Figure 15. Regimes of fluidization. Modified from (Kunii and Levenspiel, 1991)

In a fixed bed regime, a fluid is passed through a bed of particles, but the gas velocity is not enough to move the particles. In the minimum fluidization regime, the velocity is reached where all the particles are just suspended by the upward-flowing gas. The superficial velocity when reaching the minimum fluidization is the minimum fluidization velocity  $U_{mf}$ , which is defined as the velocity at which the fluid drag is equal to the weight of particles that is less than its buoyant force. With higher flow rates a bubbling fluidization is achieved, where the movement of particles is increased, and bubbles are formed but the bed doesn't expand much compared to the volume in minimum fluidization. The superficial velocity where the bed

starts to bubble is referred to as minimum bubbling velocity  $U_{mb}$ . Increasing the velocity further the size of the bubbles increases. The size of the bubble may increase to be the same size in diameter as the vessel if the vessel is deep and small in diameter. This is called slugging. With axial slugs, the fine particles flow down by the wall around the rising gas bubbles. A flat slug occurs when the bubble is as wide as the vessel, and it pushes the particles upward as it rises. Particles rain down when the slug disintegrates. (Basu, 2015; Kunii and Levenspiel, 1991)

In a turbulent fluidized bed, the terminal velocity of the solids is exceeded. The upper surface of the bed disappears, and the bed is in turbulent motion of solid clusters and voids of gas of various sizes and shapes. In the last regime of fluidization, the lean-phase fluidization with pneumatic transport as seen in Figure 15, the gas velocity is so high that the solid particles are carried out of the bed with the gas. Particle entrainment can occur in turbulent fluidized beds, but the level of entrainment is lower than in lean phase fluidization. Yerushalmi *et al.* (1976) defined that a regime between turbulent fluidized bed and the pneumatic transport of particles is a regime of fast bed fluidization. (Basu, 2015; Kunii and Levenspiel, 1991; Yerushalmi *et al.*, 1976)

CFB reactors have often been proposed for reactor type for carbonator and calciner to ensure the continuous operation with sorbent purge and replenishment (Lim *et al.*, 2023). In a CFB reactor, a bed of solid particles is fluidized by gas or liquid. The characteristics of CFBs are (Basu, 2015; Kunii and Levenspiel, 1991):

- good gas-solid mixing, that leads to close to isothermal conditions throughout the reactor
- liquidlike behavior of solid particles that allows continuous operation
- high heat and mass transfer rates between gas and particles
- well-mixed solids of the whole vessel acting as a safety buffer against rapid temperature peaks.

These characteristics provide advantages for using a CFB which are fuel flexibility, high combustion efficiency, efficient sulfur removal, and low  $\text{NO}_x$  emissions (Basu, 2015). In CFB reactors, the prevailing fluidization regimes are turbulent fluidized bed, fast fluidized bed, and pneumatic conveying (Kunii and Levenspiel, 1997). The systems for CFB are a

fluid bed that has an inner cyclone and a fast fluidized bed that has an outer cyclone. These systems are presented in Figure 16.

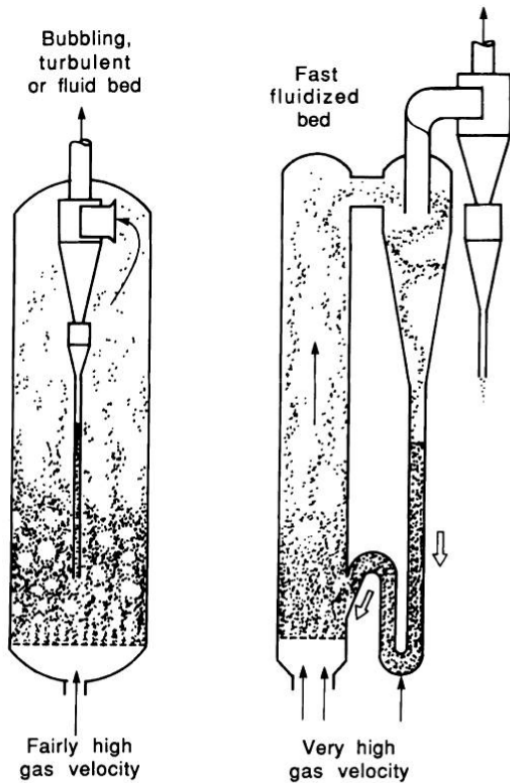


Figure 16. Turbulent and fast fluidized bed. (Kunii and Levenspiel, 1991)

The fast fluidized bed system on the right is typically the scheme that is commercially used and consequently represents the reactor type for calciner and carbonator in CaL system (See the exemplary schemes in Figure 12 and Figure 14).

#### 4.3 Loss and Deactivation of Sorbent

The sorbent is deactivated and lost in the solid looping cycle due to different mechanisms. Sintering and attrition are the main cause of the deactivation and loss of sorbent. Sulfation of sorbent material as a competing reaction to carbonation is one cause of the loss of reactive sorbent material. The deactivation of the sorbent is detected as a decrease in the sorbent  $\text{CO}_2$

carrying capacity. Make-up of the fresh sorbent is required to cover the loss and deactivation of the sorbent and the spent sorbent is collected in the purge flow. (Erans *et al.*, 2016)

In the literature, multiple equations for describing the decrease in the capacity of a sorbent material to absorb CO<sub>2</sub> in the increasing number of carbonation-calcination can be found. One of them is the semiempirical equation proposed by Grasa and Abanades (2006) presented in Equation (5). Here  $X_N$  is the sorbent carrying capacity,  $k$  is the deactivation constant [-],  $X_r$  is the residual conversion capacity and  $N$  is the number of the completed calcination-carbonation cycles. (Grasa and Abanades, 2006)

$$X_N = \frac{1}{\left(\frac{1}{1 - X_r}\right) + kN} + X_r \quad (5)$$

In Figure 17 the reactivity decay of the sorbent is presented as a function of the number of cycles calculated with  $X_r = 0.075$  and  $k = 0.52$  that have been stated to be suitable for a wide range of sorbents and conditions (Grasa and Abanades, 2006).

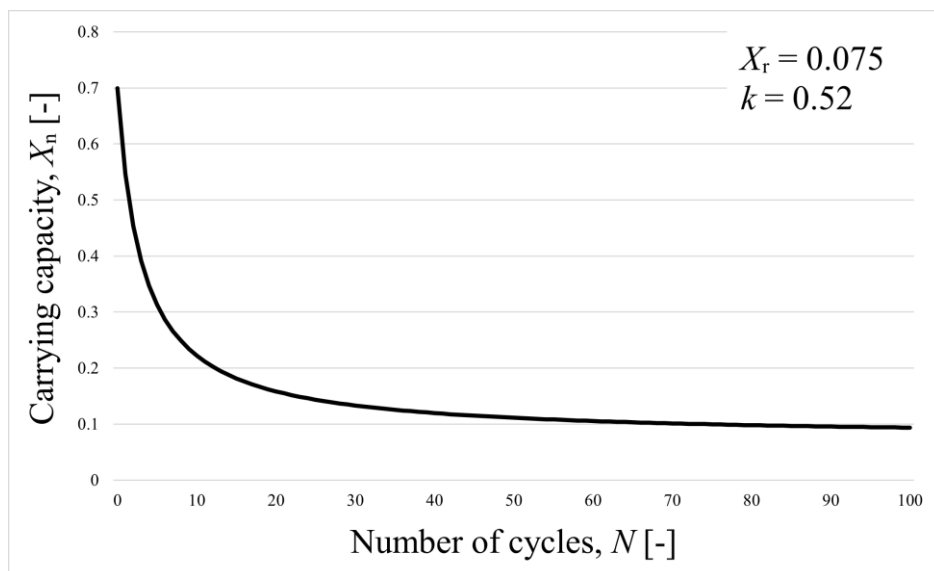


Figure 17. Sorbent deactivation as a function of number of cycles.

## Sintering

Sintering refers to a change in pore shape, grain growth, and pore size reduction due to cyclic reactions. As a result of these changes, the surface area and the reactivity of the sorbent particles decrease. Sintering accelerates in high temperatures, above 900°C, and in high partial pressures of CO<sub>2</sub> and steam which means that in the calcination step where the concentration of CO<sub>2</sub> is high, the chance for sintering is also higher. (Blamey *et al.*, 2010; Borgwardt, 1989; Wang *et al.*, 2014)

In Figure 18, Lysikov *et al.* (2007) presented a schematic diagram of the limestone sorbent behavior over the course of several carbonation-calcination cycles. Upon the first decomposition of CaCO<sub>3</sub>, a highly porous and reactive CaO is formed. The following carbonation is incomplete, due to sintering and pore blocking which leaves some unreacted CaO. During the following cycles, the amount of unreacted CaO increases until a rigid surface of CaO is formed which prevents further sintering of the sorbent.

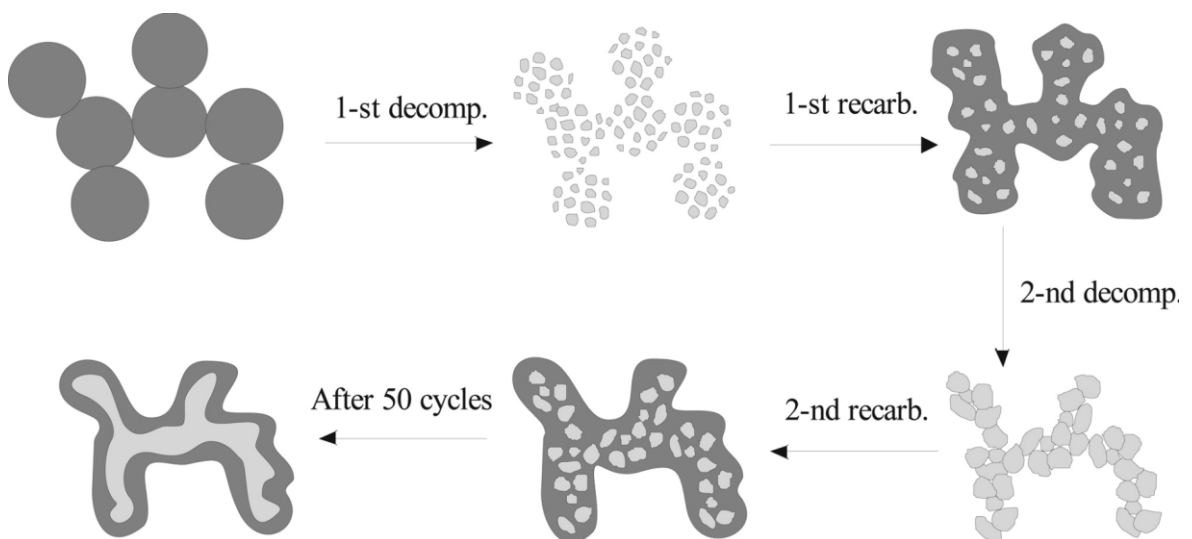


Figure 18. Schematic representation of the textural transformation of the CaO sorbent in carbonation-calcination cycles. (Lysikov *et al.*, 2007)

## Sulfation

FG contains impurities such as sulfur dioxide (SO<sub>2</sub>). CaO has a strong affinity to react with SO<sub>2</sub> under the conditions that are typical for the CaL process. Reactions with SO<sub>2</sub> cause the loss of sorbent due to CaO's reduced reactivity towards CO<sub>2</sub>. Sulfation of sorbent is a

competing reaction for carbonation in the carbonator. The sulfation occurs in the carbonator as well as in the calciner as  $\text{SO}_2$  is introduced to the calciner following oxy-fuel combustion of the supplementary fuel (Maparanyanga and Lokhat, 2021). Sulfation occurs following sulfation reactions in Equation (3) and (4).

Following both reaction paths calcium sulfate  $\text{CaSO}_4$  is formed.  $\text{CaSO}_4$  requires a higher temperature to regenerate than what is present in the CaL process, therefore it stays stable in the loop and accumulates to the system without constant purge flow. The sulfated sorbent is no longer available for absorbing  $\text{CO}_2$ .  $\text{CaSO}_4$  also causes pore blockage, due to its high molar volume. The sulfated sorbent is fed out of the process within the purge flow. (Nanda *et al.*, 2022, p. 170)

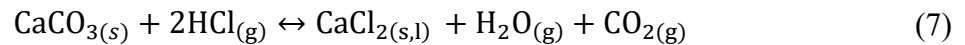
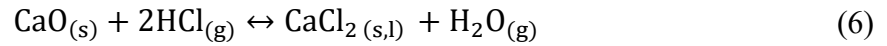
### **Attrition**

Attrition is one cause of the loss of reactive sorbent. There are different attrition mechanisms: Primary fragmentation, secondary fragmentation, and attrition by abrasion. Thermal stresses cause primary fragmentation due to the fast temperature change of particles when the sorbent is fed to a hot reactor. Thermal stress occurs during calcination when internal overpressure prevails during  $\text{CO}_2$  release from particles. Secondary fragmentation and attrition by abrasion are caused by mechanical stress. Mechanical stress is caused when particles hit each other or the walls of the reactor. Due to attrition bed particle size distribution changes and fine particles are produced that leave the cyclone with the gas stream as they are no longer efficiently separated in the cyclone. (Coppola *et al.*, 2013) Attrition rate is observed to be high at the first couple of cycles but it then decreases and stabilizes to a specific level (González *et al.*, 2010).

### **Effect of Chlorine**

Chlorine (Cl) is introduced to the CaL process as a component in the FG of the host plant and as a component of the fuel that is burned in the calciner. Fuel Cl mainly converts to hydrogen chloride (HCl) during the combustion in the calciner. The limestone-derived sorbent absorbs HCl in the temperature range of 500-650°C, which means that HCl capture occurs in the carbonator that operates at temperatures approximately 650°C. HCl absorption

is also a competing reaction to carbonation. The absorption of HCl can be described according to reactions (6) and (7). (Chyang *et al.*, 2009; Symonds *et al.*, 2021)



Calcium chloride ( $\text{CaCl}_2$ ) will decompose to CaO and HCl during calcination in the calciner which can lead to higher HCl concentrations in the product  $\text{CO}_2$  stream and in the FG path of the calciner. This can lead to potential corrosion and eventually to equipment failure if not managed appropriately. (Symonds *et al.*, 2021)

The results of Symonds *et al.* (2021) showed that the presence of steam during carbonation and calcination together with HCl can have a positive effect on the carbonation reactivity and that greater than 99% HCl capture in the carbonator can be achieved without adversely affecting sorbent  $\text{CO}_2$  capture performance. However in the case of calcination under pure  $\text{N}_2$ , carbonation conversion dropped when HCl was present without steam.

#### 4.4 Process Performance Indicators

The performance of the CaL process can be described with many indicators. Some of the essential indicators are  $\text{CO}_2$  absorption efficiency, total  $\text{CO}_2$  capture efficiency, make-up ratio, solid circulation ratio, and heat ratio.

##### **$\text{CO}_2$ Absorption Efficiency and Total $\text{CO}_2$ Capture Efficiency**

The  $\text{CO}_2$  absorption,  $E_{\text{carb}}$ , within the carbonator, is one key metric to describe the CaL process efficiency. It is a ratio between the absorbed  $\text{CO}_2$  by the sorbent and the amount of  $\text{CO}_2$  present in the FG that is introduced to the carbonator. It can be calculated according to Equation (8):

$$E_{\text{carb}} = \frac{F_{\text{CO}_2,\text{abs}}}{F_{\text{CO}_2}} = \frac{F_{\text{CO}_2} - F_{\text{CO}_2,\text{carb,out}}}{F_{\text{CO}_2}} \quad (8)$$

where  $F_{\text{CO}_2,\text{abs}}$  is CO<sub>2</sub> absorbed by the sorbent [kmol/h],  $F_{\text{CO}_2}$  is the molar flow of CO<sub>2</sub> that is introduced to the carbonator in the FG [kmol/h],  $F_{\text{CO}_2,\text{carb,out}}$  is the molar flow of CO<sub>2</sub> that is present in the FG after the carbonator [kmol/h].

The total CO<sub>2</sub> capture efficiency  $E_{\text{tot}}$  of the CaL system can be calculated according to Equation (9):

$$E_{\text{tot}} = \frac{F_{\text{CO}_2,\text{calc,out}}}{F_{\text{CO}_2,\text{carb,in}} + F_0 + F_{\text{CO}_2,\text{fuel}}} \quad (9)$$

where  $F_{\text{CO}_2,\text{calc,out}}$  is the molar flow of CO<sub>2</sub> at the calciner outlet that is fed to CPU [kmol/h],  $F_{\text{CO}_2,\text{carb,in}}$  is the molar flow of CO<sub>2</sub> that is fed to the carbonator [kmol/h],  $F_{\text{CO}_2,\text{fuel}}$  is the CO<sub>2</sub> that is released during oxy-fuel combustion of the fuel in the calciner [kmol/h] and  $F_0$  is the molar flow of CO<sub>2</sub> that is released by the first calcination of the fresh limestone make-up [kmol/h]. Total CO<sub>2</sub> capture efficiency is always higher than the CO<sub>2</sub> absorption efficiency of the carbonator because the CO<sub>2</sub> released in oxy-fuel combustion of the fuel in the calciner is captured nearly completely as well as the CO<sub>2</sub> from the first calcination of limestone.

For the CaL process that oxy-fires SRF in the calciner, 80-85% absorption efficiency in the carbonator was achieved in Haaf, Peters, et al.'s (2020) experimental study. The total capture efficiency of over 90% was achieved.

### Solid Circulation Ratio

Solid circulation ratio  $\Phi$  is an essential parameter in the CaL process. It describes the ratio between the molar flow of CaO fed to the carbonator and the molar flow of CO<sub>2</sub> introduced to the carbonator in the FG. Solid circulation ratio is calculated according to Equation (10).

$$\Phi = \frac{F_{\text{r}}}{F_{\text{CO}_2}} \quad (10)$$

The solid circulation ratio in the experimental demonstration of the CaL pilot plant using SRF in the calciner was in the range of 7.5-15. (Haaf, Peters, *et al.*, 2020)

### Make-up Ratio

The make-up ratio  $\Lambda$  of fresh sorbent to the system is typically expressed as the molar ratio between the molar flow of  $\text{CaCO}_3$  in the make-up flow and the  $\text{CO}_2$  present in the FG that is introduced to the carbonator. The make-up ratio is presented in Equation (11).

$$\Lambda = \frac{F_0}{F_{\text{CO}_2}} \quad (11)$$

The make-up ratio in the experimental demonstration of the CaL pilot plant using SRF in the calciner was in the range of 0.09-0.35. (Haaf, Peters, *et al.*, 2020)

### Heat Ratio

The heat ratio  $HR_{\text{CaL}}$  (also called as heat distribution) presents the relation of the heat supplied to the calciner to the total heat supplied to the system. It is calculated according to Equation (12).

$$HR_{\text{CaL}} = \frac{P_{\text{th,CaL}}}{P_{\text{th,tot}}} = \frac{P_{\text{th,CaL}}}{P_{\text{th,host plant}} + P_{\text{th,CaL}}} \quad (12)$$

where  $P_{\text{th,CaL}}$  is the thermal input of the fuel to calciner [MW] and  $P_{\text{th,host plant}}$  is the thermal input of the fuel to the host plant [MW].

## 5 Carbon Capture from Waste-to-Energy Plants

In this chapter the current state-of-the-art carbon capture from WtE plants is discussed. The focus is on amine-based carbon capture using monoethanolamine (MEA) which is already in commercial use in coal-fired power plants. It is often considered a benchmark carbon capture technology when different carbon capture technologies are evaluated. The CaL implementation into the WtE plant (WtE+CaL) is discussed and the topics of energy penalty, heat recovery, and heat integration are covered.

### 5.1 Current State of Carbon Capture from Waste-to-Energy Plants

There are currently several ongoing projects for carbon capture and storage from WtE plants, but commercially there is yet no full-scale WtE plant with carbon capture operating. In Oslo, Norway, The Klemetsrud project secured financing in 2022, and it is expected to be the world's first full-scale commercial CCS plant operating at a WtE plant. (NEWEST CCUS, 2022) In 2020, there were WtE+CCS plants operating on a smaller scale in Japan (Saga City), Norway (Klemetsrud, Oslo), and two plants in the Netherlands (Twence, AVR plant). All of the operating plants are based on amine absorption for post-combustion carbon capture. (IEAGHG, 2020; Wienchol *et al.*, 2020)

Pour et al. (2018) made a techno-economic and environmental impact assessment to evaluate the feasibility of WtE+CCS. The carbon capture system modeled in their study was post-combustion chemical absorption using MEA in a WtE plant that had a CFB incinerator. The results showed that WtE+CCS based on MEA has the potential for removing CO<sub>2</sub> from the FG approximately net 0.7 kg of CO<sub>2</sub>-eq per kg of wet MSW incinerated. That would accumulate to 2.8 Gt of negative CO<sub>2</sub> emissions if all the 4 Gt of MSW are treated in WtE+CCS plants annually by the year 2100. The total CO<sub>2</sub> avoided with this system was found to be 0.9 t CO<sub>2</sub>/MWh.

## MEA Integrated into WtE Plants

Magnanelli et al. (2021) investigated the integration of post-combustion CO<sub>2</sub> capture using amine absorption (MEA) into a grate-fired WtE plant producing electricity and district heat in Kristiansand, Norway. They explored various integration options, including a tail-end solution with no energy integration, heat integration with the host plant using steam extraction from the boiler, turbine, or boiler drum, and operating the capture plant only when excess heat was available. A capture efficiency of 85% was desired. The results showed that heat integration reduced the energy penalty but still with heat integration the energy penalty to the power plant was significant in all options. Without heat integration in the base case, the heat demand of the absorption plant corresponded to 27.2% of the nominal thermal capacity of the WtE plant. In the heat integration option, where the heat necessary for the capture plant was provided by steam extraction from the boiler drum, power and heat production were reduced by 30% and 6%, respectively. Similarly, steam extraction from the turbine results in an 8% reduction in power production and a 12% reduction in district heat production. It is possible to maintain 96% of the original district heat production by adjusting the condensers' temperature. Another option is to carry out carbon capture only when excess heat is available, which allows for capturing 47% of the CO<sub>2</sub> emitted by the WtE plant while reducing power production by just 5%.

The net efficiency penalty of carbon capture based on MEA in coal-fired plant was 8.7-11.4 %-points, even after process integration and minimization efforts of the net efficiency penalty (Oh *et al.*, 2018). The penalty to net efficiency of MEA in the WtE was found to be between 8.5 and 10.2 %-points in the study of Su et al. (2023), depending if heat recovery from the capture process took place or not.

## 5.2 Calcium Looping Implemented into Waste-to-Energy Plants

Although MEA has been considered a relatively mature option for post-combustion carbon capture from WtE plants as it is already commercially used in coal power plants and has been extensively developed, CaL has been proposed as a feasible alternative for post-combustion carbon capture from WtE plants.

The CaL process can be implemented into the WtE plant as a tail-end solution, which means that only the FG stream after the FG cleaning system of the host plant is fed to the CaL process and otherwise no energy streams are exchanged between the systems. However, the high-temperature heat streams in the CaL process provide an opportunity for energy integration between the host plant and the CaL system and internal energy integration within the CaL process (Lara *et al.*, 2016).

### **Energy Penalty of Calcium Looping**

The energy consumption associated with the operation of the CaL system penalizes the energy efficiency of the power plant by several percentage points if heat recovery from the excess heat streams is not performed (Lara *et al.*, 2014). However, the energy penalty of the CaL process is considered to be lower than of mature post-combustion capture technologies such as MEA (Ortiz *et al.*, 2016). The main energy penalties are associated with the heat requirements in the calciner, the oxygen separation process, and the purification and compression of captured CO<sub>2</sub> (Lara *et al.*, 2016). The possibility to heat recovery within CaL system to produce additional power is a distinctive characteristic of the CaL system, compared to other CO<sub>2</sub> capture systems (Diego *et al.*, 2017). With this additional power production, the penalty to the energy efficiency of the host plant may be decreased (Lara *et al.*, 2014).

For full-scale state-of-the-art coal-fired plants, several studies have reported the energy penalty of a CaL system via process simulations. Martínez *et al.* (2011) found that the net efficiency penalties of implementing CaL in the power plant lay between 8.3 and 10.3%-points. In the study of Hanak *et al.* (2015) the net efficiency penalty of the CaL retrofit plant was between 6.7 and 7.9 %-points. Both studies investigated a tail-end CaL solution that had a heat recovery steam generator (HRSG).

The literature lacks comprehensive studies on the energy penalty associated with the implementation of CaL in WtE plants. Haaf, Anantharaman, *et al.* (2020) conducted the first techno-economic evaluation of CaL within the context of WtE plants. The result of their study indicated that the net electrical efficiency of the WtE+CaL system can be even 5%-points higher compared to the reference WtE plant without CaL, when proper heat integration is done between CaL and the host WtE process.

Different parameters affect the process performance and therefore also to the energy penalty. After analyzing previous studies available in the literature, Hanak *et al.* (2015) stated that the fresh limestone make-up rate appears to be the key parameter affecting the process performance. The make-up rate affects the heat requirement in the calciner, as the fresh sorbent needs to be heated up to the temperature prevailing in the calciner (Rodriguez *et al.*, 2008).

### **Heat Recovery and Heat Integration**

CaL process provides high-temperature streams from which heat can be potentially recovered by the host plant. The main recoverable heat streams are (Yang *et al.*, 2010):

- heat from carbonator (heat released in exothermic carbonation reaction)
- heat from CO<sub>2</sub>-depleted FG stream from carbonator
- heat from CO<sub>2</sub> stream from calciner
- heat from the solid particles flowing from calciner to carbonator
- heat from the solid purge from the calciner

So far, solid-solid heat exchangers are more conceptual in design and not fully developed or extensively used (Papalexis *et al.*, 2023). Therefore, the heat from the solid streams may not yet be realistically viable for heat recovery.

Different ways for utilizing the recovered excess heat from the CaL process exist. The excess heat may be used internally within the CaL process to provide heat for gas and solid streams entering the calciner (Lasheras *et al.*, 2011), or to power a HRSG, an additional steam power cycle to run an additional turbine to produce electricity (Martínez *et al.*, 2011). The calciner represents a major consumer of energy in the CaL system so therefore heating up the streams entering the calciner, the energy consumption in the calciner reactor is reduced as well as the energy demand per captured tonne of CO<sub>2</sub> (Lara *et al.*, 2016). CaL is considered a tail-end solution when all the excess heat recovered is used internally in the CaL process and no heat streams are exchanged with the host process.

Heat integration with the host plant may be implemented via excess heat recovered from the CaL process to the host plant's water/steam cycle. The recovered heat from CaL can be integrated to the host plant in three different ways (Yang *et al.*, 2010):

- Use the recovered heat to provide heat for the high-pressure heaters, deaerator, or low-pressure heaters by replacing the extracted steam from the turbines that would otherwise serve these purposes in the host process.
- Use the recovered heat to provide part of the boiler heat load.
- Use the recovered heat to produce superheated steam, which can be then used to generate electricity in the turbines.

In the literature, there is still little research about heat integration of CaL and WtE plant. In Haaf, Anantharaman, et al.'s (2020) techno-economic assessment of novel heat integration concepts of CaL retrofit on a generic WtE plant, they have presented three concepts for heat integration, which are shown in Figure 19.

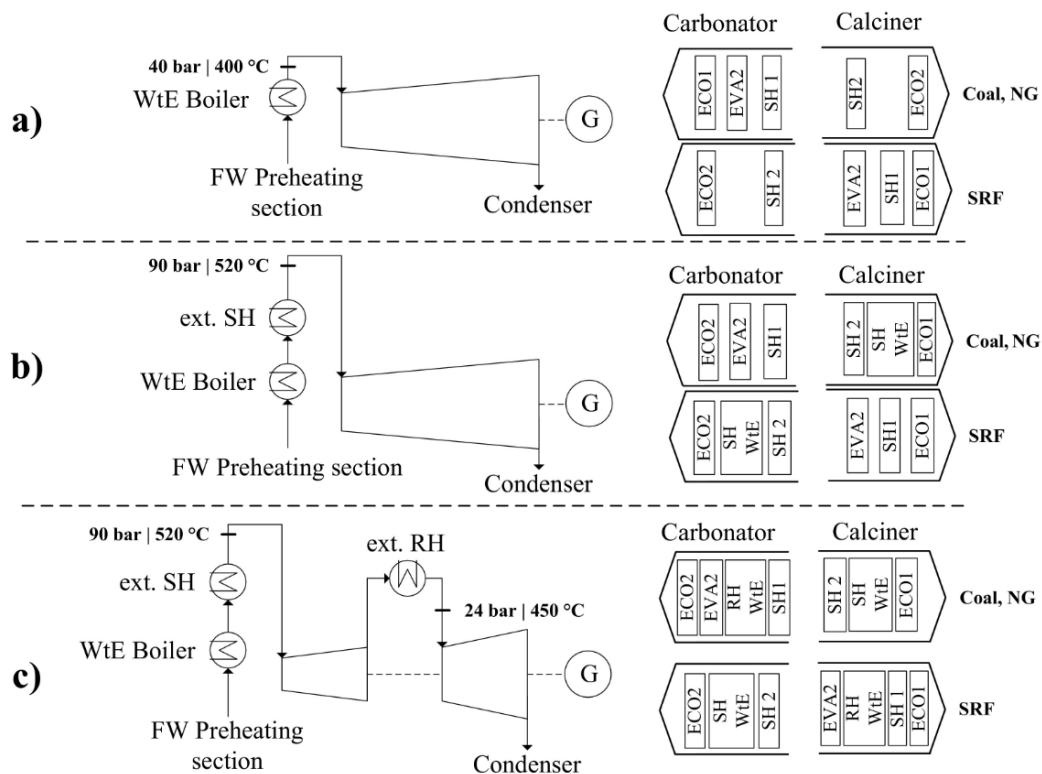


Figure 19. Heat integration concepts of CaL retrofit on a generic WtE plant and arrangement of CaL convective heat transfer surfaces with different fuels used in the calciner. Modified from (Haaf, Anantharaman, *et al.*, 2020)

Excess heat is provided both to HRSG within the CaL cycle and to the host WtE plant's power cycle. The heat integration concepts presented are the following:

- a) represents the tail-end solution where the recovered heat only powers the HRSG within the CaL cycle
- b) the recovered heat is provided to the WtE plant's power cycle for external superheating of the live steam
- c) recovered heat is provided for both external superheating and reheating of the live steam in WtE power cycle.

They noticed that the overall net electrical efficiency of WtE+CaL compared to WtE without CaL increases as the heat integration level increases. The major efficiency improvement was achieved with the concept b) of external superheating of the live steam.

## 6 Modeling of Calcium Looping Process in Aspen Plus

This chapter contains the practical part of this thesis work. The purpose is to create a simulation model in Aspen Plus to model a tail-end CaL process retrofitted to a WtE plant. Three different cases are simulated. In each case, a different fuel is considered for the calciner. The fuels that are simulated are bio-pellets, wood residue, and SRF. The focus is in presenting the heat and mass balances of the system and evaluating the effect of implementing the tail-end CaL system to the WtE plant on the CO<sub>2</sub> emissions. The impact of different fuels used in the calciner is discussed as well.

Firstly, the host WtE plant will be introduced. The basis for CaL simulation is set and a short introduction to the software Aspen Plus is given. Initial values and assumptions used for the model are presented and the model creation will be discussed in detail. Lastly, the results obtained from the three simulation cases are presented and discussed.

### 6.1 Description of the Host Waste-to-Energy Plant

The reference plant for this work is the WtE plant of Fortum Recycling & Waste located in Riihimäki, Finland. There are three combustion lines on the WtE plant site: WtE1, WtE2, and HWtE1. WtE1 and WtE2 operate grate boilers that are fed with mixed non-hazardous MSW and industrial waste. HWtE1 operates a rotary kiln boiler fed with hazardous MSW. In Table 1 the essential values for each combustion line are shown. (Fortum, 2023; Fortum Waste Solutions Oy, 2023)

Table 1. Operating values for the WtE lines of the reference plant. (SFW, 2023)

Parameter and unit	WtE1	WtE2	HWtE1
Waste input [t/a]	175000	130000	75000
Boiler duty [MW]	55	40	-
Steam pressure [bar(a)]	25	25	25
CO <sub>2</sub> output [t/a]	170748	112258	59087

Total net electricity production from the plant site is 16 MW<sub>e</sub> and total district heat production is 95 MW<sub>dh</sub>. Annual operating hours and energy outputs are summarized in Table 2. (SFW, 2023)

Table 2. Electricity and district heat production and the operating hours of the WtE plant. (SFW, 2023)

Parameter and unit	Value
Operating hours [h]	7934
Net electrical output from turbines [MW <sub>e</sub> ]	16
Total district heat output [MW <sub>dh</sub> ]	95

The FG composition and flow rates for each line are presented in Table 3. For MSW, the typical biogenic fraction is 50%, so that is considered here as a biogenic fraction for the WtE plant.

Table 3. Reference WtE plant FG composition and flowrate. (SFW, 2023)

Parameter and unit	WtE1	WtE2	HWtE1
Flowrate [Nm <sup>3</sup> /h]	119875	85146	54959
Temperature summer [°C]	117.6	53.5	125.7
Temperature winter [°C]	69.2	58.4	91.7
CO <sub>2</sub> -% wet average [%]	10.5	10.9	8.7
CO <sub>2</sub> -% wet max [%]	12.2	11.9	11.5
O <sub>2</sub> -% wet [%]	8.5	7.9	9.6
H <sub>2</sub> O-% wet [%]	16.8	21.0	19.6
SO <sub>2</sub> , average [ppm]	6.3	1.1	5.1
NO <sub>x</sub> , average [ppm]	100.0	93.5	69.3

## 6.2 Basis for Modeling of the Calcium Looping Process

In this work the CaL process is modelled in Aspen Plus as a tail-end solution to the WtE plant. As a tail-end solution, FG from all the WtE lines is fed to CaL process and no other material- or energy streams are exchanged between WtE plant and CaL process. It is further assumed that the ASU is used for the oxygen production for the CaL process. The ASU as well as the CPU are excluded from the system boundary in the simulation, so they are not modeled in this work. Instead, their evaluation relies on typical performance data derived from the literature. A generic Heat Recovery Steam Generator section (HRSG) is included to the simulation model.

### **Introduction to Aspen Plus**

Aspen Plus is a steady state chemical process simulation software that can be used to simulate various types of chemical processes. In Aspen Plus user creates flowsheets using unit operation blocks that mathematically models the functions of the block. Unit operation blocks models the specific process operations. Unit blocks may be connected in the flow-sheet to simulate an entire process system. Required information for the block is defined such as temperatures and pressures, to compute the unknown parameters, such as reaction conversion or output conditions. Aspen Plus uses an extensive physical properties database that contains physical property information on chemicals for the simulation calculations. Sequential modular approach was used in this work, which means that Aspen Plus computes the process scheme block by block. In-built functions such as Design Spec and Calculator block may be added to the model to ease the calculations. Aspen Plus enables user to also integrate user-written Fortran codes into the model. (Adams, 2022; Doherty *et al.*, 2009)

## 6.3 Model Description

The CaL process simulation model is created in Aspen Plus V12.1, (further referred as Aspen). Peng-Robinson cubic equation of state (EOS) was chosen as a physical property method. In this work the simulation contains conventional solids, nonconventional solids, and fluids and therefore in the setup of the flowsheet, the stream class is set to be

MCINCPSD. This allows fluid streams (MIXED), conventional solid streams (CIPSD), and nonconventional solid streams (NCIPSD) with particle size distribution (PSD) to be present in the simulation.

As the created simulation model is a generic description of the Cal process, some assumptions are made. The key assumptions used are listed below:

- The carbonator operates at a temperature of 650°C and the calciner operates at a temperature of 900°C.
- CFB reactors operate in atmospheric pressure (101.325 kPa).
- The separation efficiency in the cyclones is 100%.
- 95 mol.% oxygen from ASU is mixed with recirculated FG stream from the calciner to produce 50 mol.% primary oxidant for the calciner.

All the initial values and further assumptions for the CaL simulation are seen in Table 18, in Appendix 1. FG composition and flow rate (See Table 3) from the reference WtE plant is implemented into the simulation model. A yearly average temperature of the FG is applied in Aspen, and the average values of the component fractions are used. The following values in Table 4 are applied in the Aspen model.

Table 4. FG composition, temperature, and flow rate applied in the Aspen model.

Parameter and unit	WtE1	WtE2	HWtE1
Flowrate [Nm <sup>3</sup> /h]	119875	85146	54959
Temperature [°C]	93.4	55.95	108.7
CO <sub>2</sub> -% wet average [%]	10.5	10.9	8.7
O <sub>2</sub> -% wet [%]	8.5	7.9	9.6
H <sub>2</sub> O-% wet [%]	16.8	21	19.6
SO <sub>2</sub> , average [ppm]	6.3	1.1	5.1
NO <sub>x</sub> , average [ppm]	100	93.5	69.3
N <sub>2</sub>	Balance	Balance	Balance

The composition of the fuel for calciner is defined by applying the ultimate and proximate analysis. For each fuel used, the initial values for the ultimate and proximate analysis and lower heating values are seen in Table 5. Fuel and ash are defined as nonconventional solids and their density and enthalpy are calculated based on HCOALGEN and DCOALIGT enthalpy and density models, respectively. Even though the enthalpy model is HCOALGEN, the heat of combustion value is set by the user. The biogenic fraction of SRF is assumed to be 50%.

Table 5. Ultimate analysis, proximate analysis, and lower heating values of fuels

Component	Bio-pellets	Wood residue	SRF
Ultimate	wt.% <sub>dry</sub>	wt.% <sub>dry</sub>	wt.% <sub>dry</sub>
C	50.7	50.9	58.0
H	6.0	6.0	8.2
O	42.8	40.8	21.16
N	0.06	0.4	0.54
S	0.009	0.03	0.22
Ash	0.4	1.8	11.15
Cl	0.006	0.026	0.73
Proximate	wt.% <sub>dry</sub>	wt.% <sub>dry</sub>	wt.% <sub>dry</sub>
Ash	0.4	1.8	11.2
VM	72.51	78.4	81.2
FC	22.11	19.7	7.8
	wt.% <sub>ar</sub>	wt.% <sub>ar</sub>	wt.% <sub>ar</sub>
H <sub>2</sub> O	3.8	47.3	12.3
	MJ/kg <sub>ar</sub>	MJ/kg <sub>ar</sub>	MJ/kg <sub>ar</sub>
LHV	18.54	8.8	21.4

The flowsheet of the modeled tail-end CaL system is presented in Figure 20. Material flows are presented with a solid line and heat flows with a dashed line. The main reactors in the CaL system are the carbonator (CB) and the calciner (CC).

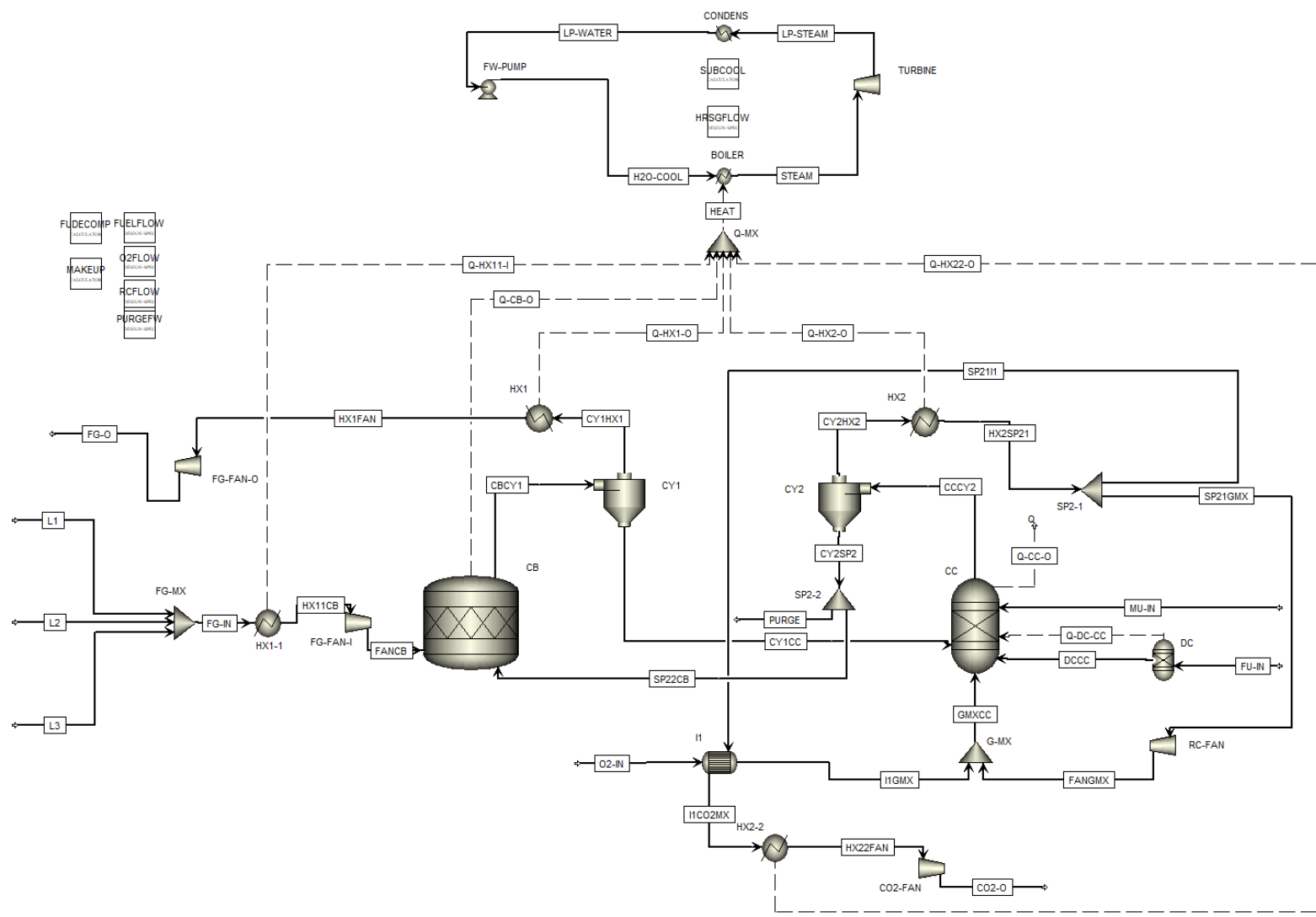


Figure 20. Flowsheet of the Aspen Plus model

The model also contains heat exchangers, cyclones, mixers and splitters, a turbine, and a pump in HRSG. The main flows entering the system are FG flow from the WtE plant entering the carbonator and flows of O<sub>2</sub>, fresh sorbent make-up, and fuel entering the calciner. The main mass flows exiting the system are CO<sub>2</sub>-lean FG exiting the carbonator's cyclone, CO<sub>2</sub>-rich gas exiting the calciner's cyclone, and solid purge flow exiting the calciner's cyclone. HRSG is a sealed loop.

The carbonation reaction is exothermic, so the carbonator is cooled to keep the temperature in the carbonator constant. This is presented as a heat stream to the HRSG. The temperature in the carbonator is kept constant at 650°C. The heat from cooling the CO<sub>2</sub>-lean gas and CO<sub>2</sub>-rich gas in the convective passes of the carbonator and the calciner is also provided to the HRSG. CO<sub>2</sub>-lean gas is cooled down to 120°C and CO<sub>2</sub>-rich gas is cooled down to a temperature of 350°C in the convective pass.

For the carbonator reactor, a block model of RStoic is used. The temperature and pressure are defined as well as reactions occurring in the carbonator. The fractional conversion of 90% for CO<sub>2</sub> is used. The carbonator's cyclone is modeled as a solid separator with complete separation of solids and vapor.

For the calciner reactor, the RGibbs model using Gibbs free energy minimization is used. The temperature in the calciner is kept constant at 900°C. As the nonconventional components do not participate in phase or chemical equilibrium calculations, a DECOMP block (RYield) is set to the flowsheet to convert the nonconventional fuel to its conventional constituents (C, H, O, N, Cl, S) to participate in phase and chemical equilibrium calculations. DECOMP block utilizes a calculator block FUDECOMP using a FORTRAN statement and the ultimate analysis of the fuel to decompose the fuel into its elements. The calciner's cyclone is defined the same way as the carbonator's cyclone described above. A split block separates part of the CO<sub>2</sub>-rich gas to be recirculated to the calciner. Oxygen and the recirculation gas are mixed in the mixer block before feeding to the calciner. The amount of recirculation gas is defined in Design Spec RCFLOW. The recirculation gas flow is varied according to the mole fraction of O<sub>2</sub> in the stream entering the calciner, which is specified to be 50%.

The amount of  $O_2$  needed in the calciner is defined by a Design Spec O2FLOW. The mole fraction of  $O_2$  in the calciner exit is defined to be 3.5%, according to which the inlet flow of  $O_2$  to the system is varied.

The fuel flow is defined in the Design Spec FUELFLOW. For the operation of the calciner, it is desired that the net heat duty of the calciner is 0 which means that the heat introduced to the calciner is in equal heat balance considering all heat sources and sinks. The fuel flow is varied in Design Spec so that the net heat duty of the calciner is 0.

The fresh sorbent make-up flow requirement is defined by the calculator block MAKEUP based on the make-up ratio (See Equation (11)). The make-up ratio used in the simulation is 0.15 and the solid circulation ratio is defined to be 8 (See Chapter 4.4). According to the solid circulation ratio, the amount of purge flow is varied in the Design Spec PURGEFW. Solid purge flow as well as the solids flow to the carbonator is separated in the separator after the calciner's cyclone.

Heat integration inside the CaL process is implemented. Excess heat from the process is provided for FG preheating before the carbonator. After the convective pass the excess heat from the  $CO_2$ -rich gas stream is made use of heating the  $O_2$  entering the calciner. The  $CO_2$ -lean gas and  $CO_2$ -rich gas are cooled down to  $120^\circ C$  before led out of the process. Solid purge flow also provides a heat source, but it is not considered for heat integration in this model.

A generic model of HRSG is connected to the CaL process. It is assumed that the simulated HRSG produces only power. The initial values used for HRSG are seen in Table 6.

Table 6. Initial values for HRSG

Parameter	Value	Reference
Live steam pressure at turbine inlet	65.2 bar	(De Lena <i>et al.</i> , 2022)
Live steam temperature	460°C	(De Lena <i>et al.</i> , 2022)
Boiler pressure drop	20 bar	(Haaf, Anantharaman, <i>et al.</i> , 2020)
Steam turbine isentropic efficiency	78.9%	(De Lena <i>et al.</i> , 2022)
Turbine mechanical efficiency	97 %	(Haaf, Anantharaman, <i>et al.</i> , 2020)
Condensation pressure	0.07 bar	(De Lena <i>et al.</i> , 2022)
Subcooling in condenser	2°C	Assumption
Pump efficiency	80%	(Haaf, Anantharaman, <i>et al.</i> , 2020)

The mass flow of feedwater is defined with a Design Spec, HRSGFLOW. The feedwater mass flow is adjusted according to the temperature of the generated steam in the evaporator which is kept constant at 460°C. A calculator block SUBCOOL is used for calculating the temperature of the low-pressure condensate after the condenser with the assumption for subcooling in the condenser of 2°C.

## 6.4 Results and Discussion

Aspen provides comprehensive stream summary tables as well as results for individual model blocks in the model once the model is successfully simulated without errors. The stream summary tables, and model results were post-processed in MS Excel.

### Carbonator Efficiency

An important matter to be verified when the results are obtained from the simulation is that the volume fraction of CO<sub>2</sub> in the carbonator is on the carbonation side of the chemical equilibrium curve (See Figure 10). The equilibrium volume fraction of the CO<sub>2</sub> in the carbonator operating temperature at 650 °C is 0.0097 according to Equation (2). The CO<sub>2</sub> volume fraction of the carbonator outlet gas in each simulation case is 0.011 which is above the

equilibrium conditions. If the molar fraction of CO<sub>2</sub> is under the chemical equilibrium curve, the assumption for the carbonator absorption efficiency must be re-evaluated. In this work, the conditions in the carbonator were on the carbonation side in all the simulation cases so no modifications to the initial values were necessary.

#### 6.4.1 Mass Balances

The complete tables for main solid and gas flows and mass balances are listed in Appendix 2. In Table 7 some of the most relevant parameters are presented and subsequently discussed.

Table 7. Key results for gas and solid flows

Parameter	Unit	Bio-pellets	Wood residue	SRF
Total CO <sub>2</sub> product gas flow rate	kg/s	33.33	49.22	36.47
Total CO <sub>2</sub> flow rate in product	kg/s	27.91	33.03	28.97
Mole fraction of CO <sub>2</sub> in product gas	mol.%	70.40%	47.17%	63.79%
Mole fraction of CO <sub>2</sub> in dry product gas	mol.% <sub>dry</sub>	92.83%	90.11%	91.43%
CaSO <sub>4</sub> content at the calciner outlet	wt.%	0.07%	0.29%	1.34%
Ash content at the calciner outlet	wt.%	0.79%	4.24%	16.03%

The total product gas flow rate is the highest in the wood residue case and the lowest in bio-pellets case, while CO<sub>2</sub> mass flow is the highest while using bio-pellets fuel. With wood residue fuel the CO<sub>2</sub> product is considerably more diluted with water vapor compared to bio-pellets and SRF case, because wood residue fuel contains the most H<sub>2</sub>O (47.3 wt.%). The difference in the CO<sub>2</sub> molar fraction in the dry product gas, which is a more essential value to be evaluated, is small between the cases. In all the cases the produced CO<sub>2</sub> product gas has more than 90% purity.

The highest ash content at the calciner outlet is observed when SRF fuel is used, that is directly due to the high ash content in SRF (See Table 5). Bio-pellets have the least amount of ash in the fuel so also the ash content in the calciner outlet is the smallest. The same phenomenon can be seen with CaSO<sub>4</sub> content in the calciner outlet: SRF contains the most sulfur, so then the CaSO<sub>4</sub> content in the calciner outlet is the largest.

### Make-up and Purge

Solid circulation ratio and make-up ratio were defined as initial values for the simulation. In Table 25 in Appendix 2 the values for mole flows for  $F_{CO_2}$ ,  $F_R$ , and  $F_0$  are presented.

The mass flow of the make-up is the same 4.96 kg/s for every fuel. The composition of the make-up, 100 wt.%  $CaCO_3$ , is also the same due to boundary conditions. In the mass flow of purge, there is some variation between the cases due to varying ash and  $CaSO_4$  content between the cases. In Table 8 the mass flows and compositions for purge flow are presented.

Table 8. Purge flow results

Purge	Unit	Bio-pellets	Wood residue	SRF
Mass flow	kg/s	2.81	2.96	3.53
CaO	wt.%	98.88	93.66	77.94
$CaCO_3$	wt.%	0	0	0
$CaSO_4$	wt.%	0.09	0.41	1.70
Ash	wt.%	1.03	5.93	20.35
Total	wt.%	100.00	100.00	100.00

The high ash and sulfur content of the SRF fuel is also seen from the purge flow composition: the mass fraction of ash and  $CaSO_4$  in purge flow are greater for SRF fuel compared to other fuel cases. No  $CaCO_3$  is present in the purge flow as complete calcination occurs under the considered calciner operation conditions.

### Oxy-fuel Combustion in the Calciner

An ASU produces  $O_2$  for the oxy-fuel combustion in a purity of 95%, the remaining 5% is assumed to be  $N_2$ . The heat ratio for each fuel is calculated according to Equation (12). The results for oxygen flow, fuel flow, specific fuel consumption, and specific  $O_2$  consumption per  $CO_2$  captured and the heat ratios are presented in Table 9.

Table 9. Fuel and oxygen flow, specific fuel and oxygen consumption, and the heat ratio in the CaL process

Parameter	Unit	Bio-pellets	Wood residue	SRF
Fuel mass flow	kg/s	7.08	18.08	7.36
Fuel input	MW <sub>LHV</sub>	131.27	159.07	157.41
Specific fuel consumption	MJ/kgCO <sub>2,capt</sub>	4.70	4.82	5.43
Carbon flow in the fuel	kmol/h	1034.67	1453.31	1121.37
O <sub>2</sub> flow from ASU (95% O <sub>2</sub> basis)	kg/s	11.02	16.06	14.61
Pure O <sub>2</sub> mass flow (100% O <sub>2</sub> basis)	kg/s	10.53	15.35	13.97
Specific O <sub>2</sub> consumption	kgO <sub>2,ASU</sub> /kgCO <sub>2,capt</sub>	0.39	0.49	0.50
Specific pure O <sub>2</sub> consumption	kgO <sub>2</sub> /kgCO <sub>2,capt</sub>	0.38	0.46	0.48
CaL process heat ratio	%	45%	49%	49%

The fuel and the oxygen consumption are the greatest for the wood residue case and smallest for bio-pellets. The mass flow of the wood residue fuel is doubled compared to other cases. On the other hand, the specific fuel consumption per captured CO<sub>2</sub> is the largest for SRF and the smallest for bio-pellets, same applies to oxygen consumption per captured CO<sub>2</sub>. The oxygen consumption is calculated based on the oxygen flow from the ASU, so the value indicates the oxygen production demand in the ASU. The reason why the O<sub>2</sub> consumption per captured CO<sub>2</sub> for bio-pellets is the smallest is that the bio-pellet fuel itself contains oxygen the most, and SRF which has the highest demand, contains the least amount of oxygen.

#### 6.4.2 Power Production of the Calcium Looping Process

The CaL process produces additional power in the HRSG section. In Table 10, the results for the HRSG section are presented. The key values are the feedwater flow, turbine gross power, generator gross power, the power consumption of the FW pump, and the total heat provided to the HRSG. The generator efficiency is 94% (De Lena *et al.*, 2022).

Table 10. HRSG results

Parameter	Unit	Bio-pellets	Wood residue	SRF
Feedwater mass flow	kg/s	35.34	43.64	41.06
Turbine gross power	MW <sub>e</sub>	33.42	41.28	38.84
Generator gross power	MW <sub>e</sub>	31.42	38.80	36.51
Total heat to HRSG	MW	114.34	141.20	132.86
FW pump consumption	MW	0.38	0.47	0.45

The total heat provided for the HRSG is the greatest in the wood residue case so accordingly also the gross power output and the cooling water demand. The FW pump consumption increases as the cooling water flow amount increases. The least gross power produced is in the bio-pellets case.

The power consumers in the CaL system modeled in this work are fans and the FW pump. The power consumption of the fans is presented in Table 11. The ASU and CPU are also major power consumers, that were not modeled, but are considered in the calculations. The values for the ASU and CPU power consumption are taken from the literature. For ASU, the specific power consumption of 200 kWh/t<sub>CO2</sub> is applied (Tranier *et al.*, 2011). It is assumed that this value presents the power consumption per tonne of the gas that ASU produces (95% O<sub>2</sub> purity). For the specific CPU power consumption a value of 115.8 kWh/t<sub>CO2</sub> is applied (Astolfi *et al.*, 2019). This is also assumed to be applied to the total CO<sub>2</sub> product stream that is led out of the CaL process in this simulation which mainly contains CO<sub>2</sub> but also other substances. The power demand of ASU and CPU are presented in Table 12.

Table 11. Fans power consumption

Fan	Unit	Bio-pellets	Wood residue	SRF
Inlet FG fan	MW <sub>e</sub>	1.25	1.25	1.25
Outlet FG fan	MW <sub>e</sub>	1.18	1.18	1.18
CO <sub>2</sub> fan	MW <sub>e</sub>	0.38	0.66	0.43
Recirculation gas fan	MW <sub>e</sub>	0.28	0.41	0.38

The flow of the FG into the carbonator as well as out of the carbonator is the same for each case. As a result, the consumptions of the FG fans are the same. The difference in fan power consumption between the cases comes in CO<sub>2</sub> and recirculation gas fans because the product CO<sub>2</sub> and recirculation gas volume flow rates are different in each case. In the wood residue case, the generation of CO<sub>2</sub> product gas is the highest, therefore, the CO<sub>2</sub> fan consumption is also the greatest. Moreover, the volume flow of the recirculation gas is the highest for wood residue so accordingly the power consumption of the recirculation gas fan is also the highest. The least power required by the fans is for the bio-pellets case.

Table 12. ASU and CPU power demand

Parameter	Unit	Bio-pellets	Wood residue	SRF
ASU power demand	MW <sub>e</sub>	7.93	11.56	10.52
CPU power demand	MW <sub>e</sub>	13.89	20.52	15.20

The power consumption of the ASU and CPU go hand in hand with the oxygen demand and the product CO<sub>2</sub> generated. The ASU and CPU power demand is the highest for wood residue as the oxygen demand is the highest and the amount of product CO<sub>2</sub> gas generated is the highest. The least power required by the ASU and CPU is for the bio-pellets case.

It is noticed that the power consumption of the CPU unit covers over 50% of the total power demand in all the cases. The share of the ASU and CPU power consumption from total power consumption is the largest in the wood residue case.

The internal power consumers are considered to obtain the net power of the CaL cycle. The net power production is calculated in two ways, including the ASU and CPU power consumption, and excluding them. The net electric efficiency of the CaL process is calculated according to Equation (13) for both cases, including and excluding the ASU and CPU power consumption. The net electric efficiency is calculated according to Equation (13).

$$\eta_e = \frac{P_e}{\Phi_f} \quad (13)$$

where  $P_e$  is the electric power [MW] and  $\Phi_f$  is the fuel input [MW]. Table 13 summarizes the net power output and electric efficiency values for the CaL system.

Table 13. Power production and efficiency results

Parameter	Unit	Bio-pellets	Wood residue	SRF
ASU&CPU included				
Net power output CaL	MW <sub>e</sub>	6.11	2.74	7.10
Net electric efficiency of CaL	%	4.66%	1.72%	4.51%
ASU&CPU excluded				
Net power output CaL	MW <sub>e</sub>	27.94	34.82	32.82
Net electric efficiency of CaL	%	21.29%	21.89%	20.85%

When all the power consumers within the CaL process are considered, the highest net power output is achieved in the SRF case. The lowest net power output is in the wood residue case. When the ASU and CPU power consumption are excluded from the net power output calculations, the highest net power output is achieved with wood residue fuel and the lowest with bio-pellets. It can be concluded that in the wood residue case, the high oxygen demand from the ASU and the high CO<sub>2</sub> product gas rate increases the ASU and CPU power demand so that compared to other fuel cases the energy penalty of the ASU and CPU is higher.

The net electric efficiency of the CaL process is low when the ASU and CPU power consumption is included. When the power consumptions of the ASU and CPU are included in net efficiency calculations, the higher energy penalty of the ASU and CPU in the wood residue case may be also detected, as the net electric efficiency is considerably lower compared to other fuel cases. The variation in net electric efficiencies when ASU and CPU are excluded is smaller between different fuels.

### Energy Penalty

As the energy products from the WtE plant and the CaL system are different (WtE produces heat and power and CaL power only), the energy penalty discussion becomes challenging. It is questionable if the efficiencies of the WtE plant and the CaL plant can be compared, or

the efficiency penalty reported. In this work, the efficiency penalty of the CaL system is not calculated. Only the net electric efficiency of the CaL plant and the additional power produced in the CaL's HRSG are reported.

In the literature, the net electrical efficiency drop of approximately 5 to 9 %-points of CaL has been achieved for power plants that produce electricity only (Martínez *et al.*, 2011; Vorrias *et al.*, 2013). The literature lacks information on the efficiency penalty of CaL retrofit to a combined heat and power (CHP) plant.

### 6.4.3 CO<sub>2</sub> Capture

The CO<sub>2</sub> that is captured originates from the FG of the host WtE plant, the oxy-fuel combustion of the calciner fuel and the first make-up limestone calcination. A balance between the origins of CO<sub>2</sub> in the system is presented in Table 14 including the parts of CO<sub>2</sub> emitted and captured from the WtE+CaL system.

Table 14. CO<sub>2</sub> balance

Parameter	Bio-pellets	Wood residue	SRF
CO <sub>2</sub> from the host WtE FG	49.50%	42.15%	47.77%
CO <sub>2</sub> from the oxy-fuel combustion in the calciner	43.08%	51.52%	45.06%
CO <sub>2</sub> from the first make-up limestone calcination	7.42%	6.32%	7.17%
CO <sub>2</sub> emitted	4.95%	4.22%	4.78%
CO <sub>2</sub> captured	95.05%	95.78%	95.22%

The portion of the CO<sub>2</sub> originating from the oxy-fuel combustion of the supplementary fuel in the calciner is approximately as large as the CO<sub>2</sub> originating from the host plants FG. For the wood residue case, the CO<sub>2</sub> generated in oxy-fuel combustion has a larger share than the CO<sub>2</sub> from the FG of the WtE plant.

The CO<sub>2</sub> absorption efficiency in the carbonator was defined to be 90% as an initial value for the simulation. The total capture efficiency  $E_{\text{tot}}$  that is calculated according to Equation (9) is 95.05%, 95.78%, and 95.22% for bio-pellets, wood residue, and SRF,

respectively, as seen in Table 14. The highest total CO<sub>2</sub> capture rate is achieved in the wood residue case, but the difference between the cases is small, less than 1%. The total capture efficiency considers all the CO<sub>2</sub> captured in the process that originates not only from the host plant FG but also from the make-up limestone and the calciner fuel. The essential stream results for CO<sub>2</sub> capture calculations are seen in Appendix 3.

In Table 15, the values for CO<sub>2</sub> emitted to the atmosphere from the WtE plant are presented. The CO<sub>2</sub> emissions are divided into biogenic emissions and fossil emissions. The biogenic fraction is subtracted from the total emitted CO<sub>2</sub>, resulting in effective CO<sub>2</sub> emission from the WtE plant.

Table 15. CO<sub>2</sub> emitted from the WtE plant

CO <sub>2</sub> emitted	Unit	Value
Total CO <sub>2</sub> emitted	kg/s	14.53
Biogenic CO <sub>2</sub> emitted	kg/s	7.27
Fossil CO <sub>2</sub> emitted	kg/s	7.27
Effective CO <sub>2</sub> emissions	kg/s	7.27

When CaL is implemented to the WtE plant, the CO<sub>2</sub> balance changes. It is considered that the CO<sub>2</sub> resulting from the oxy-fuel combustion of the supplementary fuel in the calciner is captured completely as well as the CO<sub>2</sub> resulting from the first calcination of the fresh make-up sorbent. Therefore, the CO<sub>2</sub> that is emitted to the atmosphere from the total system (WtE+CaL) is the CO<sub>2</sub> that is not captured in the carbonator. The biogenic fraction of the supplementary fuel affects the effective emissions as the biogenic fraction of the CO<sub>2</sub> that is captured is considered as negative emissions. The CO<sub>2</sub> resulting from the first calcination of the make-up is 100% fossil and doesn't affect to the effective emissions as 100% of it is captured. The total biogenic CO<sub>2</sub> captured is subtracted from the fossil CO<sub>2</sub> emitted to the atmosphere to obtain effective CO<sub>2</sub> emissions. The emitted, captured and the effective CO<sub>2</sub> emissions from WtE+CaL are presented in Table 16.

Table 16. Emitted CO<sub>2</sub> emission from WtE+CaL and effective emissions.

Parameter	Unit	Bio-pellets	Wood residue	SRF
Total CO <sub>2</sub> emitted from the carbonator	kg/s	1.45	1.45	1.45
Biogenic CO <sub>2</sub> emitted from the carbonator	kg/s	0.73	0.73	0.73
Fossil CO <sub>2</sub> emitted from the carbonator	kg/s	0.73	0.73	0.73
Total CO <sub>2</sub> captured from the WtE FG	kg/s	13.08	13.08	13.08
Biogenic CO <sub>2</sub> captured from the WtE FG	kg/s	6.54	6.54	6.54
Fossil CO <sub>2</sub> captured from the WtE FG	kg/s	6.54	6.54	6.54
Total CO <sub>2</sub> captured from the calciner fuel	kg/s	12.65	17.77	13.71
Biogenic CO <sub>2</sub> captured from the calciner fuel	kg/s	12.65	17.77	6.85
Fossil CO <sub>2</sub> captured from the calciner fuel	kg/s	0	0	6.85
Total CO <sub>2</sub> emissions	kg/s	1.45	1.45	1.45
Effective CO <sub>2</sub> emissions	kg/s	-18.46	-23.58	-12.67

The results show that the host WtE plant isn't carbon neutral or net negative without CaL implementation. The WtE plant implemented with CaL reaches net negative CO<sub>2</sub> emissions with all the alternative calciner fuels simulated in this work. The greatest net negative impact is with the wood residue fuel, but net negative CO<sub>2</sub> emissions are reached also with the SRF fuel that is partly fossil. Compared to the emissions from the WtE only, the amount of the total CO<sub>2</sub> emitted is also considerably decreased in the WtE+CaL system.

#### 6.4.4 Results Comparison to Other Studies

Some key results obtained in this work with SRF fuel are validated by comparing them to results obtained in other studies investigating CaL. A comparison is made between the values obtained in this simulation for SRF fuel and similar research done previously by Haaf, Anantharaman, et al. (2020) (referred to as Study A), also referred to earlier in this work, and research done by Vorrias et al. (2013) (referred to as Study B). In study A the first techno-economic evaluation of CaL within the context of WtE plants was conducted and process simulations were made with Aspen Plus software. Study B investigated post-

combustion carbon capture with CaL in a lignite-fired power plant with simulation software Aspen Plus and IPSEpro. The values that are compared are presented in Table 17.

Table 17. SRF results compared to previous research

Parameter	This work (Calciner fuel: SRF)	Study A (Calciner fuel: SRF)	Study B (Calciner fuel: lignite)
The CO <sub>2</sub> absorption efficiency	90%	80%	89.65%
Total CO <sub>2</sub> capture rate	95.22%	91.1%	93.93%
CaSO <sub>4</sub> content at the calciner outlet	1.34 wt.%	2.45 wt.%	-
Ash content at the calciner outlet	16.03 wt.%	20.1 wt.%	2.22 wt.%
CaL process heat ratio ( $HR_{CaL}$ )	49.1%	54.5%	36.7%
Specific O <sub>2</sub> consumption	0.48 kg <sub>O2</sub> /kg <sub>CO2,capt</sub>	-	0.336 kg <sub>O2</sub> /kg <sub>CO2,capt</sub>

The higher CaSO<sub>4</sub> content and higher ash content in study A are most likely due to the higher sulfur and ash content in the SRF fuel, than in the SRF fuel in this work. In study B the ash content of lignite fuel is considerably lower than in this work's SRF fuel. In this work,  $HR_{CaL}$  is lower than in study A and higher than in study B. The value is closer to the value obtained in study A which has similar supplementary fuel. With SRF fuel, the heat supplied to the calciner has a larger share of the total heat supplied to the system compared to the case when lignite is used as calciner fuel.

Validation of the simulation results may be done also by evaluating them based on the experimental results obtained in Haaf, Peters, et al. (2020) experimental tests of CaL firing two different SRF fuels in oxy-fuel conditions in the calciner and with FG fed to CaL that had CO<sub>2</sub> concentration typical to a WtE plant approximately 9.5-10.5 vol.%, similar to FG values in this work. In their tests, the CO<sub>2</sub> absorption efficiency of 80-85% was achieved in the carbonator which resulted in a total CO<sub>2</sub> capture rate above 90%. In the simulation of study A, where SRF was also used in the calciner, the total CO<sub>2</sub> capture efficiency was also above 90%. Considering this, the total CO<sub>2</sub> capture rate of approximately 95% achieved in the simulation in this work falls within the same range but appears to be slightly higher, which might be due to simulation model limitations, and the higher CO<sub>2</sub> absorption efficiency, and

may not fully represent the real-world CaL cycle. A large oxygen excess was required to ensure the complete conversion of the volatile matter in the SRF fuel, the excess oxygen at the calciner outlet was between 4 and 13 vol.%, average of 7.3 vol.% in the reference study. The fraction of volatile matter in the SRF fuel in this work is similar to SRF in study A, which indicates that the excess oxygen amount of 3.5 vol.% at the calciner outlet defined in this work might not be enough to ensure the complete conversion of volatile matter.

## 6.5 Further Development of the Model

The simulation model created in this work is a generic model of the CaL process. The model created in this work is sufficient for evaluating the heat and mass balances of the system. Depending on the approach for the simulation, is the desired outcome heat and mass balances or evaluation of solids behavior, for instance, the model should be further developed to achieve more accurate simulation results.

The development of the model for heat and mass balance evaluation may be started by enhancing the assumptions and adding process components that weren't added to the generic flowsheet in this work. The modeling of the ASU and CPU which were left outside the scope of this study, would be beneficial to study their effect more accurately on the system performance.

Some assumptions used in this work may cause some uncertainties in the results. It was assumed that the separation efficiency of the cyclones is 100%, which is not achieved in reality. Therefore, a more detailed model flowsheet should include also dust separation equipment, for instance, bag filters to remove the solid particles from the FG after the carbonator and from the CO<sub>2</sub> product after calciner. The make-up limestone was assumed to be 100% CaCO<sub>3</sub>, the composition could be defined more accurately in future models, as natural limestone contains also other substances. Pressure losses in pipelines could be implemented.

The current model didn't evaluate the solids behavior in the reactors, nor the reactor size or shape. In the current model the calciner was simulated at equilibrium, based on the RGibbs model block, and the carbonator was simulated with known stoichiometry and specified conversion with the RStoic block. In future modeling work more detailed reactor models may be applied. For example, Aspen Plus has a FluidBed reactor block that could be applied to

simulate the fluidized bed reactor with known reaction stoichiometry and kinetics with rigorous hydrodynamics based on the vessel design.

For more rigorous evaluation on the effect of CaL on WtE plant efficiency, part of the CaL power cycle steam could be used for heat production. In this work the efficiency penalty is not defined as the products from the WtE plant, and the CaL power cycle are different. The simulation model could be further developed by implementing the heat integration to the host plant so the efficiency penalty of the CaL could be minimized.

## 7 Summary

The objective of this work was to investigate the tail-end CaL application for decarbonizing a WtE plant. For this purpose, a literature review was conducted, and a generic simulation model of a tail-end CaL process was created in Aspen Plus. The heat integration concepts, and energy penalty of CaL were investigated based on literature review. It can be concluded that there is still little research available about CaL implementation in WtE plants.

The possibility to recover the excess heat in the CaL system to produce additional power is a distinctive characteristic of CaL. Heat integration of CaL and WtE plant may be done by means of external super- and reheating. The heat requirement in the calciner and the power consumption of the ASU and the CPU are significant factors in the energy balance of the CaL system. The additional power production in the HRSG of the CaL system and heat integration with the host plant reduce the energy penalty of the CaL. The studies about CaL as a tail-end solution to coal power plants have indicated that the efficiency penalty of CaL is between 6 and 10%-points. To the author's knowledge only one study has investigated the heat integration of CaL and WtE plants. The net electrical efficiency was found to be even 5 %-points higher for the WtE+CaL system with heat integration compared to WtE without CaL. It is evident that more research on the integration of CaL into a WtE plant needs to be conducted to better evaluate the energy penalty of CaL in the context of WtE.

Heat and mass balances as well as the power production of the CaL process and the CO<sub>2</sub> balance of the WtE+CaL system were evaluated based on the generic tail-end CaL simulation model created in the practical part of this work. The simulation model of the CaL process included the HRSG section for power production. The modeling of ASU and CPU was not performed in this work. Three cases were simulated. The supplementary fuel for calciner was different in each case, namely bio-pellets, wood residues and SRF.

According to the simulation results the specific fuel consumption and the specific O<sub>2</sub> consumption per captured CO<sub>2</sub> was found to be the greatest for the SRF fuel and lowest for bio-pellets. For bio-pellets case the specific fuel consumption was 4.70 MJ/kg<sub>CO<sub>2</sub>,capt</sub> and for SRF 5.43 MJ/kg<sub>CO<sub>2</sub>,capt</sub>. The specific O<sub>2</sub> consumptions were 0.38 kg<sub>O<sub>2</sub></sub>/kg<sub>CO<sub>2</sub>,capt</sub> for bio-pellets case and 0.48 kg<sub>O<sub>2</sub></sub>/kg<sub>CO<sub>2</sub>,capt</sub> for SRF. In terms of mass flows, wood residue required the largest O<sub>2</sub> flow from the ASU and the largest flow rate of the fuel to the calciner compared

to other cases. Make-up flow of the fresh sorbent was the same 4.96 kg/s in each case due to fixed make-up ratio of 0.15, but differences were noticed in the quantity and composition of the purge flow. The most purge flow was needed in the SRF case. The mass flow of the purge was 3.53 kg/s and the ash fraction in the purge (20.35 wt.%) was significantly larger compared to other fuels, 1.03 wt.% in bio-pellets case and 5.93 wt.% in wood residue case. That is due to higher ash content in the SRF compared to wood residue and bio-pellets. The mass flow of purge was 2.81 kg/s in bio-pellets case and 2.96 kg/s in wood residue case.

The largest CO<sub>2</sub> flow was generated in the wood residue case, with a mass flow of 33.03 kg/s while the least occurred in the bio-pellets case, with a mass flow of 27.91 kg/s. However, the CO<sub>2</sub>-richest product gas was achieved with bio-pellets where the dry molar fraction of CO<sub>2</sub> in the product gas reached 92.83 mol.%<sub>dry</sub>. Nevertheless, it's worth noting that the difference in the dry mole fraction of CO<sub>2</sub> in the product gas was small between the cases. The high ash and sulfur content of the SRF fuel was also seen in the fractions of CaSO<sub>4</sub> and ash in the calciner outlet, which were 1.34 wt.% and 16.03 wt.% respectively. The fractions were the highest for SRF fuel and the lowest for bio-pellets case, which had fractions of 0.07 wt.% and 0.79 wt.% respectively.

The highest net power output was achieved with SRF when all the power consumers within the CaL process including the ASU and CPU were considered in the calculations. The net power output in SRF case was 7.10 MW<sub>e</sub>. If the ASU and the CPU power consumption were excluded, the highest net power output was reached in the wood residue case. The ASU and CPU power demand, 11.56 MW<sub>e</sub> and 20.52 MW<sub>e</sub> respectively, was noticed to be the highest for the wood residue case because of the high oxygen demand for oxy-combustion and high CO<sub>2</sub> product gas rate.

The WtE plant alone is not carbon neutral nor net negative and half of the CO<sub>2</sub> that the WtE plant emits to the atmosphere is biogenic. With tail-end CaL implementation, the total emitted CO<sub>2</sub> as well as the fossil emitted CO<sub>2</sub> were significantly reduced, and the WtE plant reached net negative emissions in all the alternative fuel cases simulated. The negative CO<sub>2</sub> emissions were largest with wood residue fuel, -23.58 kg/s of CO<sub>2</sub>, but negative CO<sub>2</sub> emissions were reached with partly fossil SRF, -12.67 kg/s of CO<sub>2</sub>. The achieved negative CO<sub>2</sub> emissions were naturally higher for wood residue and bio-pellets, both being 100% biogenic. Therefore, based on the results obtained in this work, implementing tail-end CaL in the WtE plant contributes to climate change mitigation as a negative CO<sub>2</sub> emission technology.

## References

- Adams, T.A. (2022), *Learn Aspen Plus in 24 Hours*, Second edition., McGraw Hill, New York.
- Arias, B., Cordero, J.M., Alonso, M., Diego, M.E. and Abanades, J.C. (2013), “Investigation of SO<sub>2</sub> Capture in a Circulating Fluidized Bed Carbonator of a Ca Looping Cycle”, *Industrial & Engineering Chemistry Research*, Vol. 52 No. 7, pp. 2700–2706, doi: 10.1021/ie3026828.
- Astolfi, M., De Lena, E. and Romano, M.C. (2019), “Improved flexibility and economics of Calcium Looping power plants by thermochemical energy storage”, *International Journal of Greenhouse Gas Control*, Vol. 83, pp. 140–155, doi: 10.1016/j.ijggc.2019.01.023.
- Atsonios, K., Grammelis, P., Antiohos, S.K., Nikolopoulos, N. and Kakaras, Em. (2015), “Integration of calcium looping technology in existing cement plant for CO<sub>2</sub> capture: Process modeling and technical considerations”, *Fuel*, Vol. 153, pp. 210–223, doi: 10.1016/j.fuel.2015.02.084.
- Basu, P. (2015), *Circulating Fluidized Bed Boilers: Design, Operation and Maintenance*, 1st ed. 2015., Springer International Publishing : Imprint: Springer, Cham, doi: 10.1007/978-3-319-06173-3.
- Blamey, J., Anthony, E.J., Wang, J. and Fennell, P.S. (2010), “The calcium looping cycle for large-scale CO<sub>2</sub> capture”, *Progress in Energy and Combustion Science*, Vol. 36 No. 2, pp. 260–279, doi: 10.1016/j.peccs.2009.10.001.
- Borgwardt, R.H. (1989), “Calcium oxide sintering in atmospheres containing water and carbon dioxide”, *Industrial & Engineering Chemistry Research*, Vol. 28 No. 4, pp. 493–500, doi: 10.1021/ie00088a019.
- Bui, M., Adjiman, C.S., Bardow, A., Anthony, E.J., Boston, A., Brown, S., Fennell, P.S., *et al.* (2018), “Carbon capture and storage (CCS): the way forward”, *Energy & Environmental Science*, Vol. 11 No. 5, pp. 1062–1176, doi: 10.1039/C7EE02342A.
- Carpenter, S. and Long, H. (Eds.). (2017), “13 - Integration of carbon capture in IGCC systems”, *Integrated Gasification Combined Cycle (IGCC) Technologies*, Woodhead, Elsevier, Amsterdam, pp. 445–463.

- Chyang, C.-S., Han, Y.-L. and Zhong, Z.-C. (2009), “Study of HCl Absorption by CaO at High Temperature”, *Energy & Fuels*, Vol. 23 No. 8, pp. 3948–3953, doi: 10.1021/ef900234p.
- Coppola, A., Scala, F., Salatino, P. and Montagnaro, F. (2013), “Fluidized bed calcium looping cycles for CO<sub>2</sub> capture under oxy-firing calcination conditions: Part 1. Assessment of six limestones”, *Chemical Engineering Journal*, Vol. 231, pp. 537–543, doi: 10.1016/j.cej.2013.07.113.
- Crippa, M., Guizzardi, D., Pagani, F., Banja, M., Muntean, M., Schaaf, E., Becker, W., *et al.* (2023), *GHG Emissions of All World Countries*, Publications Office of the European Union, Luxembourg, doi: 10.2760/953332, JRC134504.
- De Lena, E., Arias, B., Romano, M.C. and Abanades, J.C. (2022), “Integrated Calcium Looping System with Circulating Fluidized Bed Reactors for Low CO<sub>2</sub> Emission Cement Plants”, *International Journal of Greenhouse Gas Control*, Vol. 114, p. 103555, doi: 10.1016/j.ijggc.2021.103555.
- Dean, C.C., Blamey, J., Florin, N.H., Al-Jeboori, M.J. and Fennell, P.S. (2011), “The calcium looping cycle for CO<sub>2</sub> capture from power generation, cement manufacture and hydrogen production”, *Chemical Engineering Research and Design*, Vol. 89 No. 6, pp. 836–855, doi: 10.1016/j.cherd.2010.10.013.
- Di Giuliano, A., Capone, S., Anatone, M. and Gallucci, K. (2022), “Chemical Looping Combustion and Gasification: A Review and a Focus on European Research Projects”, *Industrial & Engineering Chemistry Research*, Vol. 61 No. 39, pp. 14403–14432, doi: 10.1021/acs.iecr.2c02677.
- Diego, M.E. and Arias, B. (2020), “Impact of load changes on the carbonator reactor of a 1.7 MWth calcium looping pilot plant”, *Fuel Processing Technology*, Vol. 200, p. 106307, doi: 10.1016/j.fuproc.2019.106307.
- Diego, M.E., Arias, B. and Abanades, J.C. (2017), “Evolution of the CO<sub>2</sub> carrying capacity of CaO particles in a large calcium looping pilot plant”, *International Journal of Greenhouse Gas Control*, Vol. 62, pp. 69–75, doi: 10.1016/j.ijggc.2017.04.005.
- Doherty, W., Reynolds, A. and Kennedy, D. (2009), “The effect of air preheating in a biomass CFB gasifier using ASPEN Plus simulation”, *Biomass and Bioenergy*, Vol. 33 No. 9, pp. 1158–1167, doi: 10.1016/j.biombioe.2009.05.004.

- Environment Agency. (2020), “Pollution inventory reporting – incineration activities guidance note. Environmental Permitting (England and Wales) Regulations 2016 Regulation 61(1)”, Environment Agency, February.
- Erans, M., Manovic, V. and Anthony, E.J. (2016), “Calcium looping sorbents for CO<sub>2</sub> capture”, *Applied Energy*, Vol. 180, pp. 722–742, doi: 10.1016/j.apenergy.2016.07.074.
- European Commission. (2021), “Reaching new heights with CO<sub>2</sub> capture at cement plants”, available at: <https://ec.europa.eu/research-and-innovation/en/projects/success-stories/all/reaching-new-heights-co2-capture-cement-plants> (accessed 27 April 2023).
- Fawzy, S., Osman, A.I., Doran, J. and Rooney, D.W. (2020), “Strategies for mitigation of climate change: a review”, *Environmental Chemistry Letters*, Vol. 18 No. 6, pp. 2069–2094, doi: 10.1007/s10311-020-01059-w.
- Fortum. (2023), “Riihimäen laitosalue”, available at: <https://www.fortum.fi/yriyksille-ja-yhteisoille/kierratys-ja-jatepalvelut/recycling-waste-yhteystiedot-ja-toimipaikat/riihimaen-laitosalue?vtab=accordion-item-39621> (accessed 8 November 2023).
- Fortum Waste Solutions Oy. (2023), “Riihimäen laitosalue - Vuosiraportti 2022”, 27 February.
- Gasser, T., Guivarch, C., Tachiiri, K., Jones, C.D. and Ciais, P. (2015), “Negative emissions physically needed to keep global warming below 2 °C”, *Nature Communications*, Vol. 6 No. 1, p. 7958, doi: 10.1038/ncomms8958.
- González, B., Alonso, M. and Abanades, J.C. (2010), “Sorbent attrition in a carbonation/calcination pilot plant for capturing CO<sub>2</sub> from flue gases”, *Fuel*, Vol. 89 No. 10, pp. 2918–2924, doi: 10.1016/j.fuel.2010.01.019.
- Grasa, G.S. and Abanades, J.C. (2006), “CO<sub>2</sub> Capture Capacity of CaO in Long Series of Carbonation/Calcination Cycles”, *Industrial & Engineering Chemistry Research*, Vol. 45 No. 26, pp. 8846–8851, doi: 10.1021/ie0606946.
- Haaf, M., Anantharaman, R., Roussanaly, S., Ströhle, J. and Epple, B. (2020), “CO<sub>2</sub> capture from waste-to-energy plants: Techno-economic assessment of novel integration concepts of calcium looping technology”, *Resources, Conservation and Recycling*, Vol. 162, p. 104973, doi: 10.1016/j.resconrec.2020.104973.

- Haaf, M., Hilz, J., Peters, J., Unger, A., Ströhle, J. and Epple, B. (2020), “Operation of a 1 MWth calcium looping pilot plant firing waste-derived fuels in the calciner”, *Powder Technology*, Vol. 372, pp. 267–274, doi: 10.1016/j.powtec.2020.05.074.
- Haaf, M., Peters, J., Hilz, J., Unger, A., Ströhle, J. and Epple, B. (2020), “Combustion of solid recovered fuels within the calcium looping process – Experimental demonstration at 1 MWth scale”, *Experimental Thermal and Fluid Science*, Vol. 113, p. 110023, doi: 10.1016/j.expthermflusci.2019.110023.
- Hanak, D.P., Biliyok, C., Anthony, E.J. and Manovic, V. (2015), “Modelling and comparison of calcium looping and chemical solvent scrubbing retrofits for CO<sub>2</sub> capture from coal-fired power plant”, *International Journal of Greenhouse Gas Control*, Vol. 42, pp. 226–236, doi: 10.1016/j.ijggc.2015.08.003.
- Hanak, D.P., Erans, M., Nabavi, S.A., Jeremias, M., Romeo, L.M. and Manovic, V. (2018), “Technical and economic feasibility evaluation of calcium looping with no CO<sub>2</sub> recirculation”, *Chemical Engineering Journal*, Vol. 335, pp. 763–773, doi: 10.1016/j.cej.2017.11.022.
- Hein, O., Kliemke, H., Razowski, D. and Waruschewski, A. (2013), “Operating steam plant for producing electrical energy by combustion process, comprises operating electrolysis unit to provide hydrogen and oxygen, and operating methanation unit under consumption of hydrogen and carbon dioxide”, 24 October.
- Hornberger, M., Moreno, J., Schmid, M. and Scheffknecht, G. (2020), “Experimental investigation of the carbonation reactor in a tail-end Calcium Looping configuration for CO<sub>2</sub> capture from cement plants”, *Fuel Processing Technology*, Vol. 210, p. 106557, doi: 10.1016/j.fuproc.2020.106557.
- IEA. (2023a), *CO<sub>2</sub> Emissions in 2022*, International Energy Agency.
- IEA. (2023b), “Bioenergy with Carbon Capture and Storage – Analysis”, available at: <https://www.iea.org/reports/bioenergy-with-carbon-capture-and-storage> (accessed 26 April 2023).
- IEA. (2023c), “Carbon capture, utilisation and storage - Fuels & Technologies”, available at: <https://www.iea.org/fuels-and-technologies/carbon-capture-utilisation-and-storage> (accessed 26 April 2023).
- IEA Bioenergy. (2023), “Fossil vs biogenic CO<sub>2</sub> emissions | Bioenergy”, available at: <https://www.ieabioenergy.com/iea-publications/faq/woodybiomass/biogenic-co2/> (accessed 14 April 2023).

- IEAGHG. (2019), *IEAGHG, Further Assessment of Emerging CO<sub>2</sub> Capture Technologies for the Power Sector and Their Potential to Reduce Costs*.
- IEAGHG. (2020), “CCS on Waste to Energy”, 6 December.
- IPCC. (2023), *In: Climate Change 2023: Synthesis Report. Contribution of Working Groups I, II and III to the Sixth Assessment Report of the Intergovernmental Panel on Climate Change*, Geneva, Switzerland, pp. 1–34, doi: 10.59327/IPCC/AR6-9789291691647.001.
- Jayarathna, C.K., Mathisen, A., Øi, L.E. and Tokheim, L.-A. (2017), “Aspen Plus® Process Simulation of Calcium Looping with Different Indirect Calciner Heat Transfer Concepts”, *Energy Procedia*, Vol. 114, pp. 201–210, doi: 10.1016/j.egypro.2017.03.1162.
- Jeong, S., Lee, K.S., Keel, S.I., Yun, J.H., Kim, Y.J. and Kim, S.S. (2015), “Mechanisms of direct and in-direct sulfation of limestone”, *Fuel*, Vol. 161, pp. 1–11, doi: 10.1016/j.fuel.2015.08.034.
- Kaza, S., Yao, L., Bhada-Tata, P., Van Woerden, F., Ionkova, K., Morton, J., Poveda, R.A., et al. (2018), *What a Waste 2.0: A Global Snapshot of Solid Waste Management to 2050*, World Bank Group, Washington, DC, USA, doi: 10.1596/9781464813290.
- Kearns, D.T. (2019), “Waste-to-Energy with CCS: A pathway to carbon-negative power generation”, Global CCS Institute.
- Kunii, D. and Levenspiel, O. (1991), *Fluidization Engineering*, 2nd ed., Elsevier Science & Technology.
- Kunii, D. and Levenspiel, O. (1997), “Circulating fluidized-bed reactors”, *Chemical Engineering Science*, Vol. 52 No. 15, pp. 2471–2482, doi: 10.1016/S0009-2509(97)00066-3.
- Lara, Y., Lisbona, P., Martínez, A. and Romeo, L.M. (2014), “A systematic approach for high temperature looping cycles integration”, *Fuel*, Vol. 127, pp. 4–12, doi: 10.1016/j.fuel.2013.09.062.
- Lara, Y., Martínez, A., Lisbona, P. and Romeo, L.M. (2016), “Heat integration of alternative Ca-looping configurations for CO<sub>2</sub> capture”, *Energy*, Vol. 116, pp. 956–962, doi: 10.1016/j.energy.2016.10.020.
- Lasheras, A., Ströhle, J., Galloy, A. and Epple, B. (2011), “Carbonate looping process simulation using a 1D fluidized bed model for the carbonator”, *International Journal*

- of Greenhouse Gas Control*, Vol. 5 No. 4, pp. 686–693, doi: 10.1016/j.ijggc.2011.01.005.
- Leckner, B. (2015), “Process aspects in combustion and gasification Waste-to-Energy (WtE) units”, *Waste Management*, Vol. 37, pp. 13–25, doi: 10.1016/j.wasman.2014.04.019.
- Leckner, B. (2023), “Negative CO<sub>2</sub> emission from oxy-fuel combustion in CFB boilers”, *Fuel*, Vol. 333, p. 126425, doi: 10.1016/j.fuel.2022.126425.
- Leckner, B. and Gómez-Barea, A. (2014), “Oxy-fuel combustion in circulating fluidized bed boilers”, *Applied Energy*, Vol. 125, pp. 308–318, doi: 10.1016/j.apenergy.2014.03.050.
- Leckner, B. and Lind, F. (2020), “Combustion of municipal solid waste in fluidized bed or on grate – A comparison”, *Waste Management*, Vol. 109, pp. 94–108, doi: 10.1016/j.wasman.2020.04.050.
- Lim, L.H., Tan, P., Chan, W.P., Veksha, A., Lim, T.-T., Lisak, G. and Liu, W. (2023), “A techno-economic assessment of the reutilisation of municipal solid waste incineration ash for CO<sub>2</sub> capture from incineration flue gases by calcium looping”, *Chemical Engineering Journal*, Vol. 464, p. 142567, doi: 10.1016/j.cej.2023.142567.
- Liu, C., Nishiyama, T., Kawamoto, K. and Sasaki, S. (2020), “CCET guideline series on intermediate municipal solid waste treatment technologies: Waste-to-Energy Incineration”, United Nations Environment Programme, June.
- Lyngfelt, A. (2014), “Chemical-looping combustion of solid fuels – Status of development”, *Applied Energy*, Vol. 113, pp. 1869–1873, doi: 10.1016/j.apenergy.2013.05.043.
- Lysikov, A.I., Salanov, A.N. and Okunev, A.G. (2007), “Change of CO<sub>2</sub> Carrying Capacity of CaO in Isothermal Recarbonation–Decomposition Cycles”, *Industrial & Engineering Chemistry Research*, Vol. 46 No. 13, pp. 4633–4638, doi: 10.1021/ie0702328.
- Magnanelli, E., Mosby, J. and Becidan, M. (2021), “Scenarios for carbon capture integration in a waste-to-energy plant”, *Energy*, Vol. 227, p. 120407, doi: 10.1016/j.energy.2021.120407.
- Maparanyanga, T. and Lokhat, D. (2021), “Modelling of a calcium-looping fluidized bed reactor system for carbon dioxide removal from flue gas”, *International Journal of Low-Carbon Technologies*, Vol. 16 No. 3, pp. 691–703, doi: 10.1093/ijlct/ctaa102.

- Martínez, I., Grasa, G., Murillo, R., Arias, B. and Abanades, J.C. (2012), “Kinetics of Calcination of Partially Carbonated Particles in a Ca-Looping System for CO<sub>2</sub> Capture”, *Energy & Fuels*, Vol. 26 No. 2, pp. 1432–1440, doi: 10.1021/ef201525k.
- Martínez, I., Murillo, R., Grasa, G. and Carlos Abanades, J. (2011), “Integration of a Ca looping system for CO<sub>2</sub> capture in existing power plants”, *AIChE Journal*, Vol. 57 No. 9, pp. 2599–2607, doi: 10.1002/aic.12461.
- Nanda, S., Vo, D.N. and Nguyen, V.-H. (2022), *Carbon Dioxide Capture and Conversion - Advanced Materials and Processes*, Elsevier B.V., Amsterdam, Netherlands.
- Neuwahl, Frederik, Cusano, Gianluca, Gómez Benacides, Jorge, Holbrook, Simon, and Roudier, Serge. (2019), *Best Available Techniques (BAT) Reference Document for Waste Incineration*, No. EUR 29971 EN, Publications Office, LU.
- NEWEST CCUS. (2022), “Oslo’s Klemetsrud project secures financing in significant boost for waste-to-energy and CCS | NEWEST-CCUS”, *NEWEST-CCUS*, 25 March, available at: <https://www.newestccus.eu/news/oslo%E2%80%99s-klemetsrud-project-secures-financing-significant-boost-waste-energy-and-ccs> (accessed 11 May 2023).
- Oh, S.-Y., Yun, S. and Kim, J.-K. (2018), “Process integration and design for maximizing energy efficiency of a coal-fired power plant integrated with amine-based CO<sub>2</sub> capture process”, *Applied Energy*, Vol. 216, pp. 311–322, doi: 10.1016/j.apenergy.2018.02.100.
- Ortiz, C., Chacartegui, R., Valverde, J.M. and Becerra, J.A. (2016), “A new integration model of the calcium looping technology into coal fired power plants for CO<sub>2</sub> capture”, *Applied Energy*, Vol. 169, pp. 408–420, doi: 10.1016/j.apenergy.2016.02.050.
- Papalexis, C., Stefanitsis, D., Zeneli, M., Nikolopoulos, N. and Tzouganakis, P. (2023), “Proof of Concept of a Novel Solid–Solid Heat Exchanger Based on a Double L-Valve Concept”, *Energies*, Vol. 16 No. 17, p. 6156, doi: 10.3390/en16176156.
- Pour, N., Webley, P.A. and Cook, P.J. (2018), “Potential for using municipal solid waste as a resource for bioenergy with carbon capture and storage (BECCS)”, *International Journal of Greenhouse Gas Control*, Vol. 68, pp. 1–15, doi: 10.1016/j.ijggc.2017.11.007.
- Raffaini, P. and Manfredi, L. (2022), “Project management”, *Endorobotics*, Elsevier, pp. 337–358, doi: 10.1016/B978-0-12-821750-4.00015-3.

- Rodriguez, N., Alonso, M., Grasa, G. and Abanades, J.C. (2008), “Heat requirements in a calciner of CaCO<sub>3</sub> integrated in a CO<sub>2</sub> capture system using CaO”, *Chemical Engineering Journal*, Vol. 138 No. 1–3, pp. 148–154, doi: 10.1016/j.cej.2007.06.005.
- SaskPower. (2023), “Boundary Dam Carbon Capture Project”, *SaskPower*, available at: <https://www.saskpower.com/Our-Power-Future/Infrastructure-Projects/Carbon-Capture-and-Storage/Boundary-Dam-Carbon-Capture-Project> (accessed 10 May 2023).
- SFS-EN ISO 21640:2021:en. (2021), “Solid recovered fuels. Specifications and classes. (ISO 21640:2021)”.
- SFS-EN ISO 21644:2021:en. (2021), “SFS-EN ISO 21644:2021:en Solid recovered fuels. Methods for the determination of biomass content (ISO 21644:2021, Corrected version 2021-03)”.
- SFW. (2023), “Internal document - Riihimäki WtE site description”.
- Shareefdeen, Z. and Mishu, A.A. (2021), “Air emissions in waste to energy (W2E) plants”, *Clean Technologies and Environmental Policy*, doi: 10.1007/s10098-021-02049-4.
- Shimizu, T., Hirama, T., Hosoda, H., Kitano, K., Inagaki, M. and Tejima, K. (1999), “A Twin Fluid-Bed Reactor for Removal of CO<sub>2</sub> from Combustion Processes”, *Chemical Engineering Research and Design*, Vol. 77 No. 1, pp. 62–68, doi: 10.1205/026387699525882.
- Silcox, G.D., Kramlich, J.C. and Pershing, D.W. (1989), “A mathematical model for the flash calcination of dispersed calcium carbonate and calcium hydroxide particles”, *Industrial & Engineering Chemistry Research*, Vol. 28 No. 2, pp. 155–160, doi: 10.1021/ie00086a005.
- Ströhle, J., Hilz, J. and Epple, B. (2020), “Performance of the carbonator and calciner during long-term carbonate looping tests in a 1 MWth pilot plant”, *Journal of Environmental Chemical Engineering*, Vol. 8 No. 1, p. 103578, doi: 10.1016/j.jece.2019.103578.
- Su, D., Herraiz, L., Lucquiaud, M., Thomson, C. and Chalmers, H. (2023), “Thermal integration of waste to energy plants with Post-combustion CO<sub>2</sub> capture”, *Fuel*, Vol. 332, p. 126004, doi: 10.1016/j.fuel.2022.126004.
- Symonds, R.T., Lu, D.Y., Macchi, A., Hughes, R.W. and Anthony, E.J. (2021), “The effect of HCl and steam on cyclic CO<sub>2</sub> capture performance in calcium looping systems”,

- Chemical Engineering Science*, Vol. 242, p. 113762, doi: 10.1016/j.ces.2017.08.019.
- Tranier, J.-P., Dubettier, R., Darde, A. and Perrin, N. (2011), “Air separation, flue gas compression and purification units for oxy-coal combustion systems”, *Energy Procedia*, Vol. 4, pp. 966–971, doi: 10.1016/j.egypro.2011.01.143.
- UNCCS. (2019), “Climate action and support trends, United Nations Climate Change Secretariat.”
- UNEP. (2022), *Emissions Gap Report 2022: The Closing Window - Climate Crisis Calls for Rapid Transformation of Societies.*, United Nations Environment Programme, Nairobi.
- UNFCCC. (2015), “Paris Agreement”.
- U.S Department of Energy. (2017), “Secretary Perry Celebrates Successful Completion of Petra Nova Carbon Capture Project”, *Energy.Gov*, 13 April, available at: <https://www.energy.gov/articles/secretary-perry-celebrates-successful-completion-petra-nova-carbon-capture-project> (accessed 10 May 2023).
- Velis, C.A., Longhurst, P.J., Drew, G.H., Smith, R. and Pollard, S.J.T. (2010), “Production and Quality Assurance of Solid Recovered Fuels Using Mechanical—Biological Treatment (MBT) of Waste: A Comprehensive Assessment”, *Critical Reviews in Environmental Science and Technology*, Vol. 40 No. 12, pp. 979–1105, doi: 10.1080/10643380802586980.
- Vorrias, I., Atsonios, K., Nikolopoulos, A., Nikolopoulos, N., Grammelis, P. and Kakaras, E. (2013), “Calcium looping for CO<sub>2</sub> capture from a lignite fired power plant”, *Fuel*, Vol. 113, pp. 826–836, doi: 10.1016/j.fuel.2012.12.087.
- Wang, C., Zhou, X., Jia, L. and Tan, Y. (2014), “Sintering of Limestone in Calcination/Carbonation Cycles”, *Industrial & Engineering Chemistry Research*, Vol. 53 No. 42, pp. 16235–16244, doi: 10.1021/ie502069d.
- Wienchol, P., Szlęk, A. and Ditaranto, M. (2020), “Waste-to-energy technology integrated with carbon capture – Challenges and opportunities”, *Energy*, Vol. 198, p. 117352, doi: 10.1016/j.energy.2020.117352.
- Yang, Y., Zhai, R., Duan, L., Kavosh, M., Patchigolla, K. and Oakey, J. (2010), “Integration and evaluation of a power plant with a CaO-based CO<sub>2</sub> capture system”, *International Journal of Greenhouse Gas Control*, Vol. 4 No. 4, pp. 603–612, doi: 10.1016/j.ijggc.2010.01.004.

- Yerushalmi, J., Turner, D.H. and Squires, A.M. (1976), “The Fast Fluidized Bed”, *Industrial & Engineering Chemistry Process Design and Development*, Vol. 15 No. 1, pp. 47–53, doi: 10.1021/i260057a010.
- Ylätalo, J. (2013), *Model Based Analysis of the Post-Combustion Calcium Looping Process for Carbon Dioxide Capture*, Lappeenranta University of Technology, Lappeenranta, 9 December.

## Appendix 1. Initial values and assumptions for the simulation

Table 18. Initial values and assumptions for the simulation

CARBONATOR	Value	Reference
Operating temperature	650°C	(Hanak <i>et al.</i> , 2018)
Operating pressure	101.325 kPa	
CO <sub>2</sub> capture efficiency	90%	(Astolfi <i>et al.</i> , 2019)
Solid looping ratio	4-14, (8 used in this work)	(Hornberger <i>et al.</i> , 2020)
FG preheating	120°C	
CALCINER		
Operating temperature	900°C	(Hanak <i>et al.</i> , 2018)
Operating pressure	101.325 kPa	
Excess O <sub>2</sub> in calciner off CO <sub>2</sub> -stream	3.5 vol.%	
Oxygen concentration at calciner inlet	50 %	(Astolfi <i>et al.</i> , 2019)
Gas temperature at convective pass outlet	350°C	(Astolfi <i>et al.</i> , 2019)
MAKE-UP		
- temperature	25°C	
- pressure	101.325 kPa	
- purity	100 % of CaCO <sub>3</sub>	
- make-up ratio	0.05-0.24, (0.15 used in this work)	(Ströhle <i>et al.</i> , 2020)
FUEL		
- temperature	25°C	
- pressure	101.325 kPa	
O <sub>2</sub> -INLET		
- pressure	120 kPa	
- temperature	25°C	
- oxygen purity	95 vol.% O <sub>2</sub> 5 vol.% N <sub>2</sub>	(Astolfi <i>et al.</i> , 2019)
- O <sub>2</sub> preheating temperature	170°C	

CO <sub>2</sub> outlet temperature	120°C	
Recycled CO <sub>2</sub> temperature	350°C	(Astolfi <i>et al.</i> , 2019)
Gas-gas heat exchangers minimum temperature approach	10°C	(Hanak <i>et al.</i> , 2015)
Pressure drops		
- Heat exchangers	10 mbar	(Jayarathna <i>et al.</i> , 2017)
- Carbonator	90 mbar	
- Calciner	90 mbar	
- Gas phase in convective pass	35 mbar	(Haaf, Anantharaman, <i>et al.</i> , 2020)
- Cyclones	10 mbar	(Jayarathna <i>et al.</i> , 2017)
Pressure increase		
- Inlet FG fan	0.1 bar	
- Outlet FG fan	0.1 bar	
- CO <sub>2</sub> fan	0.1 bar	
- Recirculation fan	0.135 bar	
Fans		
- Isentropic efficiency	0.85	
- Mechanical efficiency	0.95	

## Appendix 2. Stream results for main solid and gas flows

Table 19. Main gas flows. Wood residue

		FG to CaL	CB In	CB Out	CC In	CC Out	O <sub>2</sub> inlet	Rec Gas	CO <sub>2</sub> out
Temperature	°C	60.70	131.74	650	282.09	900	25	350	130.64
CO <sub>2</sub>	mol.%	10.25	10.25	1.13	23.20	47.17	0.00	47.17	47.17
H <sub>2</sub> O	mol.%	18.77	18.77	20.67	23.43	47.65	0.00	47.65	47.65
N <sub>2</sub>	mol.%	62.44	62.44	68.78	3.36	1.67	5.00	1.67	1.67
O <sub>2</sub>	mol.%	8.54	8.54	9.40	50.00	3.50	95	3.50	3.50
SO <sub>2</sub>	ppm	4.343	4.343	4.785	0.0275	0.0559	0	0.0559	0.0559
CH <sub>4</sub>	ppm	0	0	0	0	0	0	0	0
CO	ppm	0	0	0	0.0112	0.0227	0	0.0227	0.0227
HCL	ppm	0	0	0	21.60	43.91	0	43.91	43.91
H <sub>2</sub>	ppm	0	0	0	0.00897	0.0182	0	0.0182	0.0182
CL <sub>2</sub>	ppm	0	0	0	0	0	0	0	0
Mass flow	kg/s	90.59	90.59	77.51	31.18	64.34	16.06	15.12	49.22
Mole flow	kmol/h	11599.02	11599.02	10528.96	3577.79	7486.98	1818.22	1759.57	5727.41

Table 20. Main gas flows. Bio-pellets

		FG to CaL	CB In	CB Out	CC In	CC Out	O2 inlet	Rec Gas	CO <sub>2</sub> out
Temperature	°C	60.70	131.74	650	284.31	900	25	350	130.17
CO <sub>2</sub>	mol.%	10.25	10.25	1.13	34.62	70.40	0	70.40	70.40
H <sub>2</sub> O	mol.%	18.77	18.77	20.67	11.88	24.15	0	24.15	24.15
N <sub>2</sub>	mol.%	62.44	62.44	68.78	3.49	1.94	5	1.94	1.94
O <sub>2</sub>	mol.%	8.54	8.54	9.40	50.00	3.50	95	3.50	3.50
SO <sub>2</sub>	ppm	4.343	4.343	4.785	0.0275	0.0559	0	0.0559	0.0559
CH <sub>4</sub>	ppm	0	0	0	0	0	0	0	0
CO	ppm	0	0	0	0.0167	0.0339	0	0.0339	0.0339
HCL	ppm	0	0	0	6.29	12.79	0	12.79	12.79
H <sub>2</sub>	ppm	0	0	0	0.00455	0.00925	0	0.00925	0.00925
CL <sub>2</sub>	ppm	0	0	0	0	0	0	0	0
Mass flow	kg/s	90.59	90.59	77.51	23.43	45.74	11.02	12.41	33.33
Mole flow	kmol/h	11599.02	11599.02	10528.96	2454.92	4450.15	1247.58	1207.34	3242.82

Table 21. Main gas flows. SRF

		FG to CaL	CB In	CB Out	CC In	CC Out	O <sub>2</sub> inlet	Rec Gas	CO <sub>2</sub> out
Temperature	°C	60.70	131.74	650	283.66	900	25	350	130.31
CO <sub>2</sub>	mol.%	10.25	10.25	1.13	31.37	63.79	0	63.79	63.79
H <sub>2</sub> O	mol.%	18.77	18.77	20.67	14.87	30.23	0	30.23	30.23
N <sub>2</sub>	mol.%	62.44	62.44	68.78	3.69	2.35	5	2.35	2.35
O <sub>2</sub>	mol.%	8.54	8.54	9.40	50.00	3.50	95	3.50	3.50
SO <sub>2</sub>	ppm	4.343	4.343	4.785	0.0275	0.0559	0	0.0559	0.0559
CH <sub>4</sub>	ppm	0	0	0	0	0	0	0	0
CO	ppm	0	0	0	0.0151	0.0307	0	0.0307	0.0307
HCL	ppm	0	0	0	632.9	1286.9	0	1286.9	1286.9
H <sub>2</sub>	ppm	0	0	0	0.00569	0.0116	0	0.0116	0.0116
CL <sub>2</sub>	ppm	0	0	0	0.0595	0.121	0	0.121	0.121
Mass flow	kg/s	90.59	90.59	77.51	30.33	52.19	14.61	15.72	36.47
Mole flow	kmol/h	11599.02	11599.02	10528.96	3254.79	5315.52	1654.07	1600.72	3714.80

Table 22. Main solid flows. Wood residue

		Make-up	CB out / CC in	CB in	Fuel	Purge	CC out
Mass flow	kg/s	4.96	171.28	158.20	18.08	2.96	161.16
Temperature	°C	25	650	900	25	900	900
CaO	wt.%	0	76.77	93.66	0	93.66	93.66
CaSO <sub>4</sub>	wt.%	0	0.38	0.41	0	0.41	0.41
Ash	wt.%	0	5.48	5.93	0	5.93	5.93
Fuel	wt.%	0	0	0	100	0	0

Table 23. Main solid flows. Bio-pellets

		Make-up	CB out / CC in	CB in	Fuel	Purge	CC out
Mass flow	kg/s	4.96	162.93	149.85	7.08	2.81	152.65
Temperature	°C	25	650	900	25	900	900
CaO	wt.%	0	80.71	98.88	0	98.88	98.88
CaSO <sub>4</sub>	wt.%	0	0.08	0.09	0	0.09	0.09
Ash	wt.%	0	0.95	1.03	0	1.03	1.03
Fuel	wt.%	0	0	0	100	0	0

Table 24. Main solid flows. SRF

		Make-up	CB out / CC in	CB in	Fuel	Purge	CC out
Mass flow	kg/s	4.96	203.18	190.10	7.36	3.53	193.64
Temperature	°C	25	650	900	25	900	900
CaO	wt.%	0	64.72	77.94	0	77.94	77.94
CaSO <sub>4</sub>	wt.%	0	1.60	1.71	0	1.71	1.71
Ash	wt.%	0	19.05	20.36	0	20.36	20.36
Fuel	wt.%	0	0	0	100	0	0

Table 25. Values for  $F_{CO_2}$ ,  $F_R$  and  $F_0$  obtained from simulation results

	Bio-pellets [kmol/h]	Wood residue [kmol/h]	SRF [kmol/h]
$F_{CO_2}$	1188.96	1188.96	1188.96
$F_R$	9511.65	9511.59	9511.67
$F_0$	178.34	178.34	178.34

Table 26. Mass balance. Wood residue

IN			OUT		
		[kg/s]			[kg/s]
Gas	FG	90.59	Gas	Carbonator	77.51
	O <sub>2</sub>	16.06		Calciner	49.22
Solid	Fuel	18.08	Solid	Purge	2.96
	Make-up	4.96			
Total		129.69	Total		129.69

Table 27. Mass balance. Bio-pellets

IN			OUT		
		[kg/s]			[kg/s]
Gas	FG	90.59	Gas	Carbonator	77.51
	O <sub>2</sub>	11.02		Calciner	33.33
Solid	Fuel	7.08	Solid	Purge	2.81
	Make-up	4.96			
Total		113.65	Total		113.65

Table 28. Mass balance. SRF

IN			OUT		
		[kg/s]			[kg/s]
Gas	FG	90.59	Gas	Carbonator	77.51
	O <sub>2</sub>	14.61		Calciner	36.47
Solid	Fuel	7.36	Solid	Purge	3.53
	Make-up	4.96			
Total		117.52	Total		117.52

### Appendix 3. Stream results for CO<sub>2</sub> capture

Table 29. Stream results for CO<sub>2</sub> capture

		Bio-pellets	Wood residue	SRF
$F_{\text{CO}_2,\text{carb},\text{out}}$	kmol/h	118.90	118.90	118.90
$E_{\text{carb}}$	%	90.00	90.00	90.00
$\text{CO}_2,\text{carb},\text{out}$	mol.%	0.01	0.01	0.01
$\text{CO}_2,\text{carb}$	kg/s	13.08	13.08	13.08
$\text{CO}_2,\text{make-up}$	kg/s	2.18	2.18	2.18
$\text{CO}_2,\text{fuel}$	kg/s	12.65	17.77	13.71
Total captured CO <sub>2</sub>	kg/s	27.91	33.03	28.97
Carbonation	%	46.87	39.61	45.15
Limestone	%	7.81	6.60	7.53
Supplementary fuel	%	45.32	53.79	47.32
Total	%	100.00	100.00	100.00

Table 30. Stream results for total CO<sub>2</sub> capture

		Bio-pellets	Wood residue	SRF
$F_{\text{CO}_2,\text{calc},\text{out}}$	kmol/h	2283.07	2701.71	2369.79
$F_{\text{CO}_2,\text{carb},\text{in}}$	kmol/h	1188.96	1188.96	1188.96
$F_{\text{CO}_2,\text{fuel}}$	kmol/h	1034.67	1453.31	1121.37
$F_0$	kmol/h	178.34	178.34	178.34
$E_{\text{tot}}$	%	95.05	95.78	95.22